C. elegans synMuv B proteins regulate spatial and temporal chromatin compaction during development

Meghan E. Costello[1], Lisa N. Petrella[1]*

[1]Department of Biological Sciences, Marquette University, Milwaukee, WI 53233, USA

*Correspondence: lisa.petrella@marquette.edu

Keywords: H3K9me2, chromatin, gene repression, synMuv B, temperature stress

Summary Statement

C. elegans synMuv B proteins regulate chromatin compaction preceding upregulation of zygotic gene expression to ensure proper gene repression and cell fate decisions, especially at high temperature.

Abstract

Tissue-specific establishment of repressive chromatin through creation of compact chromatin domains during development is necessary to ensure proper gene expression and cell fate. *C. elegans* synMuv B proteins are important for the soma/germline fate decision and mutants demonstrate ectopic germline gene expression in somatic tissue, especially at high temperature. We show that *C. elegans* synMuv B proteins regulate developmental chromatin compaction and that timing of chromatin compaction is temperature sensitive in both wild-type and synMuv B mutants. Chromatin compaction in mutants is delayed into developmental time-periods when zygotic gene expression is upregulated and demonstrates an anterior-to-posterior pattern. Loss of this patterned compaction coincides with the developmental time-period of ectopic germline gene expression that leads to a developmental arrest in synMuv B mutants. Finally, accelerated cell division rates at elevated temperature may contribute to a lack of coordination between expression of tissue specific transcription programs and chromatin compaction at high temperature. Thus, chromatin organization during development is regulated both spatially and temporally by synMuv B proteins to establish repressive chromatin in a tissue-specific manner to ensure proper gene expression.

Introduction

Generating proper chromatin organization during development is required for fate specification. As cells go from a totipotent one-cell zygote to a multicellular differentiated organism, chromatin transitions from being highly dynamic and non-ordered to being more static, with clear euchromatic and heterochromatic domains within the nucleus (Mutlu et al., 2018; Politz et al., 2013; Yuzyuk et al., 2009). These changes in chromatin are concurrent with the developmental transition from no/very low zygotic gene expression to zygotic, fate-specific gene expression (Levin et al., 2012; Robertson and Lin, 2015; Spencer et al., 2011). Closed or compacted chromatin domains are often associated with genes that demonstrate low/no expression. Chromatin compaction is thought to have an influence on the level of gene expression by in part regulating the ability of transcription factors and polymerase to have access to genes (Elgin and Reuter, 2013; Simon and Kingston, 2013).

Repressive chromatin domains are formed during early embryogenesis (Gonzalez-Sandoval, et al., 2015; Motlu et al., 2018; Politz et al., 2013; Yuzyuk et al., 2009). There are two types of canonical repressive chromatin, constitutive heterochromatin that covers gene poor and repeat rich regions of the genome, and facultative heterochromatin that is found in gene rich regions of the genome and acts as a spatial-temporal regulator of gene repression (Ahringer and Gasser, 2018; Latorre et al., 2015). *C. elegans* have holocentric chromosomes with gene rich, active centers and gene poor, repeat rich arms (Ahringer and Gasser, 2018; Albertson and Thomson, 1982; Gerstein et al., 2010). Constitutive heterochromatin is found along chromosome arms in *C. elegans,* and facultative heterochromatin can be found in the more euchromatic centers of chromosomes (Liu et al., 2011; Evans et al., 2016). Although these classical designations of repressed chromatin have been characterized in worms, it has become increasingly clear that chromatin dynamics are complex and cannot always be classified into these two designations (Ahringer and Gasser, 2018; Liu et al., 2011). Repressive chromatin is established in active regions of the genome by tissue specific mechanisms in other organisms, but the regulators and establishment of facultative heterochromatin

during crucial developmental windows for proper fate specification have yet to be elucidated (Gaertner et al., 2012; Smolko et al., 2018).

synMuv B proteins are a group of conserved transcriptional repressors important in the tissue specific repression of a large set of genes. Loss of a subset of synMuv B proteins, including members of the DREAM complex, LIN-15B, and MET-2, results in the ectopic expression of germline genes in the somatic intestine (Andersen and Horvitz, 2007; Petrella et al., 2011; Wang et al., 2005; Wu et al., 2012). Gene misexpression in the intestine leads to High Temperature L1 larval Arrest (HTA) in DREAM complex and *lin-15B* mutants (Petrella et al., 2011). The DREAM complex and LIN-15B bind to the promoter regions of target genes throughout the genome where they are thought to repress their expression (Goetsch et al., 2017, Rechtsteiner et al., 2019). The highly conserved DREAM complex has eight known subunits including LIN-35 and LIN-54 (Fay and Yochem, 2007; Harrison et al., 2006). LIN-35, the single worm homolog of the mammalian pocket protein retinoblastoma, mediates the interaction of the subcomplex portions of the DREAM complex, and in it its absence the DREAM complex has highly reduced binding and repression capabilities (Goetsch et al., 2017). LIN-54 acts as one of the DNA binding subunits of the DREAM complex and in its absence the DREAM complex is lost from 80-90% of target loci (Tabuchi et al., 2011). LIN-15B has not been shown to be part of the DREAM complex, but demonstrates the same phenotypes as seen in DREAM complex mutants, including ectopic germline gene expression and HTA (Petrella et al., 2011). MET-2 catalyzes mono- and di-methylation of histone H3 lysine 9 (H3K9me1 and H3K9me2), a histone modification associated with repressive chromatin (Andersen and Horvitz, 2007; Towbin et al., 2012). *met-2* mutants lose ~80% of H3K9me2 (Towbin et al., 2012). Although loss of the DREAM complex, LIN-15B, or H3K9me2 catalyzed by MET-2 all lead to ectopic expression of germline genes, the role and order of each of these proteins during development remains unknown.

The phenotypes demonstrated by synMuv B mutants are temperature sensitive. Larval arrest only happens at high temperature and ectopic germline gene expression is more extensive at high temperatures (Petrella et al., 2011). Chromatin has been shown to be affected by changes in temperature in other organisms. For example, early studies in *Drosophila* revealed that high temperature causes incomplete polytene heterochromatin formation (Hartmann-Goldstein, 1967). Additionally, work in plants has shown that flowering time is linked to changes in chromatin that occur in response to increased temperature (Zografos and Sung, 2012). Therefore, the temperature sensitivity of synMuv B mutants may be associated with temperature sensitivity of chromatin. We hypothesized that synMuv B proteins regulate gene expression at the chromatin level throughout development and are particularly necessary for the proper chromatin regulation and buffering of gene expression during temperature stress.

Here we investigate the loss of synMuv B proteins on chromatin compaction during development and during times of temperature stress. The temperature sensitivity of chromatin in *C. elegans*, and its regulating proteins, has never been examined in a developmental context before this study. We report that the timing of chromatin compaction during embryogenesis based on cell number is delayed at high temperatures, even in wild-type embryos. We demonstrate that synMuv B mutants have an increased amount of open chromatin, both in general chromatin assays and at specific germline gene loci, especially at high temperature. We find the delay in chromatin compaction in synMuv B mutants occurs in an anterior posterior pattern. This patterned developmental delay occurs during the temperature sensitive periods for the high temperature arrest phenotype and ectopic germline gene expression. Our data support a mechanism that synMuv B proteins are necessary to regulate the proper spatial and temporal formation of repressive chromatin throughout development to promote fate-specific gene expression programs.

Results

synMuv B proteins regulate developmental chromatin compaction

Loss of the histone H3 K9 (H3K9me1/2) mono- and di-methyltransferase *met-2* results in loss of ~80-90% of H3K9me2 and delayed general chromatin compaction during development (Fakhouri et al., 2010; Mutlu et al., 2018; Yuzyuk et al., 2012). As H3K9me2 localization to synMuv B target genes is lost in the soma of *lin-15B* mutants, and to a lesser extent in *lin-35* mutants (Rechtsteiner et al., 2019), we investigated if chromatin compaction is compromised more broadly in synMuv B mutants. To assess general chromatin compaction during development, we utilized the Nuclear Spot Assay (Fakhouri et al., 2010; Yuzyuk et al., 2009). The Nuclear Spot Assay uses an extrachromosomal array containing numerous *lacO* sites that are bound by a ubiquitously expressed GFP-LacI protein. This assay has been previously utilized in *C. elegans* to visualize chromatin compaction throughout development as differentiation is achieved (Gonzalez-Sandoval et al., 2015; Yuzyuk et al., 2009). We visualized chromatin compaction in intestinal cells in wild-type, *lin-15B, lin-35, lin-54,* and *met-2* mutants at three embryonic stages and in L1 larvae at 20°C and 26°C. These specific embryonic stages were chosen based on the state of zygotic gene expression and ease of staging. First, 8E embryos have eight intestinal cells and represent an early embryonic stage (~50-100 cell embryo), where the zygotic gene expression program has yet to be fully activated. Second, 16E embryos have sixteen intestinal cells and represent a mid-embryonic stage (~150-200 cell embryo), where zygotic gene expression has been upregulated. Finally, comma stage embryos have twenty intestinal cells and represent a mid-to-late embryonic stage (>200 cells), where zygotic gene expression is fully underway (Fig. 1A). We scored intestinal cells as having either open arrays, which have a de condensed floret or crescent shape within the nucleus, or closed arrays, which have a tight ellipse/puncta shape within the nucleus, to determine differences between strains and temperatures (Fig. 1B) (Yuzyuk et al., 2009). In wild-type embryos we observed that at 20°C by the 8E stage, chromatin was already in a primarily compact state in intestinal cells (Fig. 1C). However, in wild-type at 26°C at the 8E and 16E stages, we saw that there were significantly more intestinal nuclei that

displayed open arrays, but that by comma stage were closed (Fig. 1C). This suggests that temperature causes a delay in developmental chromatin compaction even in a wild-type state.

In all four synMuv B mutants at 20°C at the 8E stage, we saw that there were significantly more intestinal nuclei with open arrays compared to wild-type embryos at 20°C (Fig. 1C). However, for all synMuv B mutants at 20°C by the 16E stage, there were very few intestinal cells with open arrays, and only in *lin-35* mutants was the number of cells with open arrays significantly higher than wild-type at 20°C (Fig. 1C). At 26°C, mutants show a more drastic delay in chromatin compaction displaying significantly more open arrays through all stages, except for *lin-54* and *met-2* mutants at the L1 stage (Fig. 1C). Furthermore, we saw that within an individual mutant background at 26°C compared to 20°C, there were significantly more intestinal nuclei with open arrays at each stage of development, except for *met-2* mutants at the L1 stage (Fig. 1C). Overall, synMuv B mutant intestinal cells showed a developmental delay in compaction at 26°C compared to 20°C, and at high temperature, compaction was delayed into developmental stages where zygotic gene expression has started.

To confirm our scoring method, we performed 3-D volumetric analysis of the intestinal nucleus measuring the volume of an array compared to the volume of the nucleus. Open arrays should take up more volumetric space; and therefore, have a larger array volume to nuclear volume ratio. 3-D volumetric data showed similar trends to those described above; intestinal cells had a larger array volume to nuclear volume ratio in mutants vs. wild-type, and at 26°C vs. 20°C (Fig. 1D, E). In contrast to the open/closed scoring in wild-type at 26°C compared to 20°C, even at stages where we scored most or all of the arrays as closed, we saw a small but significant increase in the array volume to nuclear volume ratio (Fig. 1E). This indicated that arrays take up a variable amount of nuclear volume even when they appear compacted. In mutants, there was a striking increase in not only the percent of nuclear volume taken up by the array compared to wild-type, but also an increased in the variance of the array volume within the same genotype, especially at 26°C. In general, as development proceeded,

mutant cells show a decreased array volume to nuclear volume ratio, decreased variance of array volume within a genotype, and a significant difference between temperatures (Fig. 1E). Overall, the 3-D volumetric analysis supports our open/closed data as we see a temperature sensitive chromatin compaction phenotype throughout development, predominantly in synMuv B mutants.

Wild-type embryos show a rate of cell division to each developmental stage in at 26°C

Developmental speed increases at elevated temperatures based on for the first cell division and time to hatching (Begasse et al., 2015, Wood et al., 1980). However, the developmental timing of the intestinal lineage has not been described at 26°C. The delay in chromatin compaction in wild-type embryos at 26°C compared to 20°C at 8E and 16E may be due to chromatin compaction requiring a minimum absolute time to occur while cell division rates can be accelerated. To test this hypothesis, we measured the time to each stage of intestinal development based on E cell number at 20°C and 26°C. To perform these timing experiments, 2 cell embryos expressing a fluorescent intestinal cell marker were dissected from gravid adults, plated at 20°C or 26°C, and observed throughout development. The time in minutes were recorded for each embryo as they reached 8E, 16E, comma, pretzel, and L1 stages. We found that the time to 8E in wild-type embryos was on average 3.9 hours at 20°C and 3.09 hours at 26°C (Fig. 2). The decreased developmental time in wild-type embryos was observed at all stages, as embryos plated at 26°C reach each division approximately an hour before embryos plated at 20°C (Fig. 2; Table S1, Table S2). Thus, the absolute time at which an embryo reached 8E or 16E was significantly earlier at 26°C versus 20°C.

synMuv B mutants have delayed development compared to wild-type embryos

We found that synMuv B mutants have open chromatin in later stages of development, especially at high temperature. To determine if synMuv B mutants have delayed chromatin compaction due to changes in the overall rate of embryonic development, we observed the time to each intestinal division at 20°C and 26°C for *lin-15B* and *lin-54* mutants using the same methods as described above for wild type. If

synMuv B mutants had a much faster rate of cell cycle compared to wild type at a given temperature, than that could explain a delay in chromatin compaction into stages of later intestinal development. However, instead synMuv B mutants were slower to each intestinal division when compared to wild-type embryos (Fig. 2). synMuv B mutants reached a specific developmental intestinal stage an average of 30 and 21 minutes (*lin-15B* and *lin-54* respectively) after a wild-type embryo reached the same stage at the same temperature (Fig. 2; Table S1, Table S3). The developmental delay in reaching each embryonic cell stage based on intestinal cell number in synMuv B mutants stayed relatively constant throughout embryonic development (Fig. 2, Table S3). However, like wild type embryos, synMuv B mutant embryos also showed accelerated development of a about one hour less time to each stage at 26°C compared to 20°C (Fig. 2, Table S2). Thus, loss of chromatin compaction in synMuv B mutants was not explained by an acceleration of cell division rate in mutants compared to wild type embryos, but accelerated development at 26°C may explain their even further delay in chromatin compaction seen at elevated temperatures.

There is not a delay MET-2 localization in *lin-15B* mutants

The timing of general chromatin compaction during development is concordant with the increased nuclear localization of MET-2 (Mutlu et al., 2018). Therefore, if the timing of MET-2 nuclear localization is delayed in *lin-15B* or DREAM complex mutants this could lead to a delay in chromatin compaction. We looked at the localization of MET-2:FLAG at in *lin-15B* mutants to determine if mutants could have a delay MET-2 nucluer localization beyond the 8E stage. *lin-15B* mutants demonstrated normal MET-2 nuclear accumulation when compared to wild-type embryos with clear accumulation of MET-2 by ~50 cell stage right, which should be near the beginning of the 8E stage (Fig. S1).

Individual embryos contain nuclei with both open chromatin and closed chromatin

While scoring array compaction we observed that population wide, the number of intestinal cells with open arrays decreases gradually through development in mutants. For example, in pooled *lin-15B* mutant intestinal cells at 26°C at the 16E stage about

50% of the cells contain open arrays (Fig. 1C). We wanted to determine if, at a particular stage of development, the partial compaction seen in the population of intestinal cells was due primarily to variance in compaction of individual intestinal cells within an embryo (Fig. 3A: Model 1) or variance in compaction of intestinal cells between different embryos (Fig. 3B: Model 2). If model 1 is supported, we would expect to see a population of embryos with a mosaic of open and closed cells within each embryo. If model 2 is supported, we would expect to see a binary distribution of embryos within the population containing either all open or all closed intestinal cells. We found that in a population of embryos, each embryo contained a mix of intestinal cells with both open and closed arrays that was close to the population mean (Fig. 3C). For example, in *lin-15B* mutants at 26°C at 8E, when about 90% of intestinal cells were scored as open (Fig. 1C), embryos have a range of 6/8 to 8/8 cells with open arrays. While at 16E, when about 50% of intestinal cells were scored as open (Fig. 1C), *lin-15B* mutant embryos have between 6/16 and 10/16 cells with open arrays. We did not find a genotype or temperature with a bimodal distribution where the embryos within a population fell into a mix of 100% closed and 100% open arrays. This data supports model 1. As development proceeded and chromatin compaction was achieved, the number of open cells within an embryo decreased. The pattern of compaction within an embryo was similar between mutant genotypes at the same stage and temperature (Fig. 3C).

synMuv B proteins regulate chromatin compaction spatially in an anterior-to-posterior direction

While scoring the number of open cells within an embryo, we observed an anterior-to-posterior pattern of chromatin compaction. The intestinal cell lineage descends from a single cell, E. The first cell division is an anterior-posterior division in which E becomes 2E. These two intestinal cells divide in a left-right division (2E to 4E) to establish the bilateral symmetry of the intestine. The resulting cells are designated as sister cells with a set consisting of a left and right pair. The third division when 4E gives rise to 8E is an anterior-posterior division although the cells are slightly displaced in the dorsal-ventral plane (Fig. 4A, sister cells labeled as a', c', e', f'). The 4th division is an anterior-

posterior division that gives rise to 16E with some cells more dorsal than others (Fig. 4B, sister cells labeled as a, b, c, d, e, f, g, h). The sixteen cells subsequently polarize and change shape before there is a final round of cell division in which only the most anterior pair of sister cells (a) divide in a dorsal-ventral direction, and the most posterior pair of sister cells (h) divide in an anterior-posterior direction leading to the final arrangement of cells within the nucleus (Fig. 4C, sister cells labeled a, a'', b, c, d, e, f, g, h, h''). We found that there was a clear pattern in the anterior-posterior location of cells with open arrays within an embryo. At 8E when mutants have varying numbers of cells open at 20°C and 26°C, we found that the anterior pair of sister cells maintained open arrays more often in all four genotypes, while the most posterior cells most often had closed arrays (Fig. 4). For example, at 20°C, when *lin-15B* mutants have a range of 2/8 to 8/8 cells open, the a' sister cells were open 100% of the time. The following pair of sister cells, f', had the next highest percentage of open cells (90%). The more posterior sister cells, c', have a decreasing number of open cells (60%), and the two most posterior sister cells, h', have the lowest percentage of open cells (30%) (Fig. 4A). This pattern of open arrays being more often in the anterior and less often in the posterior was observed in all four mutants, at 8E, 16E, and comma stages, at both 20°C and 26°C (Fig. 4). Overall if an embryo had any intestinal cells with an open array, they were always the cells found at the anterior section of the intestine (Fig. 4). This suggests that as development proceeds and chromatin compaction is achieved, cells close in a posterior to anterior direction. This pattern seems to be independent of proliferative state, as there is a final cell division at both anterior and posterior positions to give rise to 20E (Fig. 4C a and a'', h and h'')

synMuv B proteins regulate compaction of chromosomal germline gene loci

To determine if chromatin compaction is also altered at chromosomal loci whose expression is regulated by synMuv B proteins, we performed fluorescent *in-situ* hybridization (FISH). It Pairs of red and green probes ~100kb apart were created to flank endogenous loci to determine the level of compaction at those loci (Yuzyuk et al., 2009). All loci assessed were located in central regions of autosomes that are generally euchromatic to control for autosomal location. As controls we used the *pha-4* gene that

should be open and expressed in the intestine, and the *myo-3* gene that should be closed and not expressed in the intestine (Ardizzi and Epstein, 1987; Horner et al., 1998). We investigated three synMuv B regulated genes *ekl-1*, *coh-3*, and C05C10.7, which are germline genes that are upregulated in synMuv B mutants (Petrella et al., 2011). Intestinal cells were imaged in 3-D stacks at the 8E, 16E, and comma stage, and we calculated the level of chromatin compaction of the loci based on the 3-D distance between the centroid of each probe (Yuzyuk et al., 2009). We found that, as predicted, the non-expressed *myo-3* control locus was more compact than the expressed *pha-4* control locus in all genotypes at both temperatures in all embryonic stages (Fig. 5A and B, Fig. S2). The *myo-3* locus demonstrated compaction reminiscent of compaction of extra-chromosomal arrays, which are also not expressed (Fig. 5A and B, Fig. S2). In wild-type at 20°C *myo-3* is completely compacted by the 8E stage (Fig. 5A and B, Fig. S2). However, in wild-type at 26°C, there was a significant difference in the level of compaction of the *myo-3* locus between the 8E and 16E stages, representing a delay in compaction timing compared to 20°C (Fig. 5A and B, Fig. S2). Thus, although there may be slight delays in chromatin compaction of an unexpressed locus at elevated temperatures or in mutants, cellular mechanisms can overcome these delays by late embryogenesis.

We next analyzed the three synMuv B target genes (*ekl-1, coh-3, C05C10.7),* which have higher expression in mutants than wild-type and higher expression at 26°C within mutants (Petrella et al., 2011). In wild-type, all three of these loci showed similar patterns to the *myo-3* locus with loci reaching maximal compaction between the 8E or 16E stage at both temperatures (Fig. 5A and B, Fig. S2). Thus, in wild-type at both 20°C and 26°C the synMuv B target loci showed a pattern of compaction like a non-expressed locus. However, in synMuv B mutants the three targets genes showed two different patterns of developmental compaction depending on the temperature being assayed. In synMuv B mutants at 20°C at the 8E stage the *ekl-1, coh-3*, and C05C10.7 loci were all less compacted than the same locus in wild-type, but showed wild type levels of compaction by the comma stage (Fig. 5A). Thus, at 20°C the three synMuv B regulated loci showed a delay in compaction but by late embryo genesis were as

compact as in wild-type. On the other hand, in synMuv B mutants at 26°C the three synMuv B target loci were more open than the same locus in wild-type at all developmental stages (Fig. 5B). In *lin-35, lin-54,* and *met-2* mutants, both the *coh-3* and C05C10.7 were as open as the *pha-4* locus in the same genotype (Fig. 5B, Fig. S2). Thus, synMuv B target loci demonstrate a level of chromatin compaction similar to highly expressed genes late into development, but only at 26°C. The presence open chromatin around synMuv B targets during later developmental time periods at high temperature may leave these genes vulnerable to the ectopic misexpression found in synMuv B mutants.

16E through comma stage is the critical developmental time-period for larval high temperature arrest in synMuv B mutants

synMuv B mutants arrest at the L1 larval stage, which is at least in part due to ectopic expression of germline genes (Petrella et al*.,* 2011). To determine if the developmental time-period important for the HTA phenotype is consistent with embryonic stages in which we see prolonged open chromatin, we performed temperature shift experiments on *lin-15B, lin-35, lin-54,* and *met-2* mutants. Previous studies determined that the temperature-sensitive period for HTA is in a broad developmental range during embryogenesis and early larval development (Petrella et al*.,* 2011), but did not look at specific embryonic stages. To perform HTA experiments, 4-cell embryos expressing a fluorescent intestinal cell marker were dissected from gravid adults and downshifted or upshifted at 4E, 8E, 16E, comma, pretzel and L1 developmental stages. Pretzel stage was included as an easily distinguishable later developmental stage to tease apart differences seen in worms shifted at comma and L1. Wild-type embryos were also dissected and shifted at all stages and never arrested (data not shown). All mutant embryos upshifted to 26°C from 20°C at 4E or 8E arrested at the L1 stage (Fig. 6A-D). When upshifted at 16E all mutant genotypes except *lin-15B* showed a slightly fewer arrested animals than at earlier stages (Fig. 6A-D). A smaller number of embryos upshifted at comma and pretzel stages arrested (Fig. 6A-D). Finally, embryos upshifted at the larval L1 stage did not arrest (Fig. 6A-D). Together, embryos shifted early in development arrested whereas embryos shifted in mid-to-late embryogenesis

sometimes arrested, suggesting the critical time period for HTA to be after 16E. We also performed downshift experiments to hone in on the developmental window crucial for HTA. Embryos downshifted from 26°C to 20°C at 4E did not arrest and about half of embryos downshifted at 8E arrested (Fig. 6A-D). Strikingly most embryos downshifted at 16E and comma arrested (Fig. 6A-D). And downshifting at pretzel and L1 stages caused 100% arrested at the larval L1 stage (Fig. 6A-D). These data combined suggest 16E through comma is the most crucial temperature sensitive time-period for HTA. However, upshifting after or downshifting before this time-period can still cause some animals to undergo HTA, suggesting a buffering in the system that may represent stochastic chromatin compaction, varying amounts of ectopic gene expression, and a leaky arrest phenotype.

Downshifting from 26°C to 20°C at the pretzel or L1 stages resulted in 100% larval arrest (Fig. 6A-D), suggesting that gene misexpression programs leading to HTA are activated and their effects are irreversible. Although it was previously reported that HTA was irreversible upon downshifting, whether germline genes continued to be ectopically expressed after downshift was not assessed (Petrella et al., 2011). We set out to determine if germline gene ectopic expression was at similar levels after downshift and in worms that continually experienced 26°C. We analyzed the level of the germline specific P-granule protein PGL-1 by using strains with the endogenous *pgl-1* locus tagged with GFP (Andralojc, et. al., 2017). *pgl-1* is a synMuv B regulated germline gene that has been used to show ectopic germline gene expression in synMuv B mutants (Petrella et al., 2011, Wang et al., 2005, Wu et al., 2012). *lin-15B* and *lin-54* mutant embryos were downshifted at 8E, 16E, and comma stage and imaged at the L1 stage to determine the level of ectopic PGL-1 expression. We found that L1s downshifted as embryos resembled L1s kept at 26°C at all stages with no significant difference in average maximum fluorescent intensity (Fig. 6E-G, Fig. S3). There was a significant difference when comparing shifted embryos and those kept at 26°C to mutant embryos raised at 20°C (Fig. 6E-G, Fig. S3). Because GFP protein is a long-lived protein it cannot be determine if the level of PGL-1::GFP seen in L1s represents actively ongoing PGL-1 expression or previously expressed protein. However, as the PGL-1::GFP

expression level was indistinguishable between L1s grown continually at 26°C and those down-shifted from 26°C to 20°C, those embryos down-shifted during embryonic development at a minimum reached higher levels of expression than those embryos kept continually at 20°C. This suggests that the ectopic gene expression program that leads to HTA was activated in early embryogenesis under temperature stress and that the effects of this misexpression are irreversible.

Discussion

Chromatin compaction during development is necessary to achieve proper gene expression and differentiation. Previous studies have identified that H3K9 methylation is essential for chromatin compaction and organization (Ahringer and Gasser, 2017; Mutlu et al., 2018; Towbin et al., 2012). Although methylation of H3K9 is necessary, the pathways and proteins needed to establish areas of compaction in a tissue specific way remain unclear. Here we show that synMuv B proteins are necessary for timely chromatin compaction during development. Loss of any of these proteins; the DREAM complex DNA binding protein LIN-54, the pocket protein that helps maintian the DREAM complex binding LIN-35, LIN-15B, or the H3K9me1/2 methyltransferase, MET-2, causes impaired chromatin compaction and ectopic germline gene expression in early development. This suggests that binding of LIN-15B, the DREAM complex, and methylation of H3K9 are each necessary for proper repression at germline gene loci in somatic tissue. Loss of any one of these proteins causes ectopic expression of germline genes and improper organismal development during temperature stress.

Methylation of H3K9 is necessary to achieve chromatin compaction at the right time and place during development. Loss of MET-2 causes loss of ~80% of H3K9me1/2 across the genome. Previous studies have shown that *met-2* mutants ectopically express germline genes and have reduced embryonic chromatin compaction (Fakhouri et al., 2010; Towbin et al., 2012). We have shown that *met-2* mutants also demonstrate the HTA phenotype (Rechtsteiner et al., 2019). Interestingly, the DREAM complex binds only ~1400 and LIN-15B binds to ~2100 locations throughout the genome, primarily on

autosomes (Goetsch et al., 2017; Latorre et al., 2015; Rechtsteiner et al., 2019). Loss of LIN-15B or DREAM binding, at relatively few places throughout the genome, causes the same phenotypes as losing ~80% of H3K9me1/2. One explanation for this similarity is that LIN-15B and the DREAM complex may be tissue specific regulators of H3K9 methylation at synMuv B regulated loci and this modification may be important for repression of germline genes in somatic tissue (Rechtsteiner et al., 2019). Another explanation is that loss of individual mechanisms that contribute to closed chromatin; broad H3K9me2 or DREAM complex/LIN-15B regulation at specific loci, each lead to an increased temperature sensitivity of compact chromatin formation globally. Therefore, the similarity in phenotype is secondary consequence to general changes in chromatin compaction at many loci across the genome. Further analysis of the interaction of the DREAM complex/LIN-15B with MET-2 and H3K9me2 are needed to distinguish these possibilities.

Chromatin is found in a generally unorganized and open state early in development (Politz et al., 2013; Yuzyuk et al., 2009). As development proceeds and differentiation occurs, chromatin becomes compacted and organized in a tissue specific manner (Mutlu et al., 2018; Politz et al., 2013; Yuzyuk et al., 2009). Organization of chromatin within the nucleus generally precedes upregulation of zygotic gene expression and is important for correct cell fate decisions (Gaertner et al., 2012; Mutlu et al., 2018; Politz et al., 2013; Yuzyuk et al., 2009). Because poised Pol II accumulates at promoters in a developmental stage specific, but not tissue specific manner (Gaertner et al., 2012), upregulation of gene expression during the maternal-to-zygotic switch occurs globally throughout the embryo (Gaertner et al., 2012). Therefore, establishment of tissue specific repression, including establishment of repressive chromatin, must occur before global gene expression is upregulated to achieve cell fate specific expression patterns (Gaertner et al., 2012; Poliltz et al., 2013; Yuzyuk et al., 2009). Loss of synMuv B proteins leads to global changes in chromatin compaction into the developmental time of the maternal-to-zygotic switch, especially at high temperature, leaving their target loci vulnerable to expression when zygotic gene expression is upregulated. synMuv B mutants demonstrate three different temperature sensitive phenotypes; ectopic germline

gene expression, delayed chromatin compaction, and HTA. Because changes in chromatin compaction and gene expression are so intimately linked it is difficult to distinguish the more primary of these phenotypes. It may be that synMuv B protein binding blocks the access of transcription factors or Pol II binding/activation to synMuv B target loci. Thus, in the absence of these synMuv B proteins these genes are ectopically expression, which in turn leads to a loss of chromatin compaction. On the other hand, synMuv B proteins may help establish repressive chromatin environments before the maternal-to-zygotic switch, such that when synMuv B proteins are mutated the cell experiences inability to compact chromatin, especially at synMuv B target loci. In this case, it is the loss of compaction that allows these genes to be expressed either through changes in activator accessibility or the conformational changes to the chromatin that allows for active transcription. Because chromatin compaction can eventually reach wild type levels in synMuv B mutants at 20°C, despite the near complete loss of DREAM complex binding and H3K9me2 at germline gene promoters (Goetsch et al., 2017; Rechtsteiner et al., 2019), temperature appears to be a key of both increased gene misexpression and loss of chromatin compaction.

The synMuv B phenotypes of delayed chromatin compaction, ectopic germline gene expression, and HTA are all temperature sensitive (Petrella et al., 2011). However, this temperature sensitivity is not likely due to misfolding of mutant proteins or complex disassociation missing a member. First, even mutants that produce no protein, like *lin-35(n745)* and *lin-15B(n744)*, demonstrate temperature sensitivity. Second, the binding of the DREAM complex is significantly impaired in both *lin-35(n745)* and *lin-54(n2231)* mutants even at 20°C. Finally, double mutants between different components of the pathway, for example *lin-15B; met-2* or *lin-15B; lin-35,* do not demonstrate enhanced phenotypes at lower temperatures (M.E.C., unpublished data). Therefore, it appears that there is something about temperature effects on the broader system that are integral to these phenotypes. Early studies in *Drosophila* revealed that high temperature causes incomplete heterochromatin formation (Hartmann-Goldstein, 1967). Our data in wild type embryos indicates that formation of closed chromatin may require a minimum absolute time to occur, which is demonstrated by the delay in chromatin

compaction to later developmental stages when cell division rates are accelerated at high temperature. In synMuv B mutants the loss of a single protein/complex that helps to reorganize chromatin into compact domains results in a short delay in chromatin compaction compared to wild type at 20°C, but compensatory mechanisms by redundant players appear to allow for generally normal development. That synMuv B mutants take longer to reach each developmental stage compared to wild type may aid in coordination of formation of closed chromatin and up-regulation of zygotic gene expression in the mutants at 20°C. However, synMuv B mutant embryos, similar to wild type embryos, take ~60 minutes less time to reach each stage of development at 26°C versus 20°C. Therefore, the increase in cell cycle speed combined with a slowed rate of formation of compact chromatin formation in synMuv B mutants at 26°C may result in disruption of the coordination in the timing of compact chromatin formation, and either Pol II activation or transcription factor binding during development. This lack of coordination may be the primary cause of failure of synMuv B target loci to compact chromatin, ectopic gene expression, and ultimately HTA at elevated temperature.

The experiments performed here were all done with a high temperature condition at the end of the temperature range where laboratory experiments are routinely done for *C. elegans*. This raises the question of whether these temperature stresses reflect levels that these organisms would experience under more natural conditions. Work in the last 10-15 years has greatly expanded our understanding of the ecology of naturally occurring *C. elegans* populations (Schulenburg and Felix, 2017). Unlike what was previously thought, it is now known that the reproductive lifespan and embryogenesis of *C. elegans* occur at the soil surface, often within rotting plant vegetation (Felix and Duveau, 2012; Frezal and Felix, 2015; Kiontke et al., 2011). In our temperature shift experiments, a window of 6-8 hours within embryogenesis at 26°C elicited a severe chromatin delay in developing embryos resulted in HTA in mutants. Given the short time-period needed, it seems likely, that there are circumstances where *C. elegans* embryos in natural habitats would experience the temperatures tested here. Thus, having mechanisms that ensure that chromatin compaction occurs during the correct developmental window at these temperatures would be necessary for species survival.

We found that delayed chromatin compaction in synMuv B mutants demonstrated an anterior-to-posterior pattern within intestinal cells. The anterior cells of the intestine were the last to adopt closed chromatin, a pattern independent of replication capacity, as there is a both final anterior and posterior division to form the *C. elegans* intestine. The *C. elegans* intestine is patterned anteriorly to posteriorly by Wnt signaling proteins (Fukushige et al., 1996; Lin et al., 1998; Schroeder and McGhee, 1998). Wnt signaling associated transcription factors are loaded into the most anterior cells of the intestine at each division (Schroeder and McGhee, 1998). It is possible that anteriorly loaded transcriptional factors are able to ectopically bind and express vulnerable germline genes in the anterior intestine leading to high temperature arrest.

One of the hallmark phenotypes of synMuv B mutants is the ectopic expression of germline genes in the soma. It is important to understand how germline genes are repressed in somatic tissue as many human somatic cancers that are highly proliferative and metastatic show upregulation of germline genes (Gure et al., 2005; Maine et al., 2016; Xu et al., 2014). Like *C. elegans*, mammals also repress germline gene expression during embryogenesis in somatic cells and recent work has indicated that this repression is dependent on H3K9me2 (Ebata, et. al., 2017; Lian et. al., 2018). Given that the DREAM complex is completely conserved between worms and mammals (Litovchick, et al., 2007), its role in establishment of developmental repressive chromatin at germline genes may also be conserved. Further studies of synMuv B regulation will provide evidence of how organisms establish and maintain chromatin structure and gene expression states to ensure vitality.

Materials and Methods

Strains and nematode culture

C. elegans were cultured on NGM plates seeded with *E. coli* strain AMA1004 at 20°C unless otherwise noted. N2 (Bristol) was used as wild-type. Strain LNP0050 containing the transgene bnEx80(68xlacO+myo-3::mCherry+worm genomic DNA); gwls39[baf-1p::GFP::lacI::let-8583\'UTR;vit-5::GFP];caIs79(elt-2p::dTomato;pRF4)) was created for this study and crossed into mutant worms. Mutant alleles used were *lin-15B(n744), lin-35(n745), lin-54(n2231), lin-37(n758),* and *met-2(n4256).* Strain EL364 has a CRISPR tagged *3XFlag::met-2* (Mutlu et al., 2018). The complete strain list can be found in Table S2.

Nuclear Spot Assay

Wildtype and mutant embryos and L1s with *gwls39[baf-1p::GFP::lacI;;let-858 3\'UTR; vit-5::GFP]; bnEx85 (68xlacO+myo-3::mcherry+genomic C05C10.7+worm genomic DNA)* and *caIs79[elt-2p::dTomato, pRF4 (rol-6+)]* arrays were collected and fixed with methanol and acetone and mounted using Gelutol (Petrella et al., 2011). Each genotype was scored at 8E, 16E, comma, and L1. High temperature samples were collected by upshifting L4 P0 worms to 26°C before collecting F1 embryos or L1s. L1 larvae were obtained by hatching embryos in the absence of food in M9 buffer. Images were acquired in Z-stacks using a Nikon A1R laser scanning confocal unit controlled by NIS-Elements fitted on a Nikon inverted Eclipse T*i-E* microscope with a Nikon DS-Qi1Mc camera and Plan Apo 100X/1.4 numerical aperture oil objective. For chromatin compaction analysis, each intestinal cell's array was scored by eye as either open or closed as described in Yuzyuk *et al,* 2009. Briefly, arrays that had a hazy, distended, floret or crescent configuration were scored as "open" as this morphology suggest these arrays were partially de-compacted. As development proceeded, arrays became compacted and gained a clear, tight, ellipsoid morphology. These ellipsoid arrays were scored as "closed" as this suggested globally compacted and repressed arrays. Nuclear volumetric array compaction analysis was performed using the isosurface function in Metamorph V7.8.8.0. ND2 files were opened in Metamorph, a rectangular

box was drawn around a single embryo, and the stack was opened in 4D viewer. Inclusive threshold and the isosuface function were used to create a mask of the two channels selected: the red intestinal cells and the green arrays. Each individual intestinal cell and array was selected, and the volume was calculated using the measure function. Specifically, the volume of both the nucleus and GFP+ LacO arrays of each individual intestinal cell was measured and used to determine the percentage of the nucleus that the array represented. Statistical analysis was performed by 2-way ANOVA using Prism Graph Pad.

embryo E cell location lacO array scoring

Embryos scored for chromatin compaction analysis were also scored for percentage of open cells within an embryo. The intestinal cells at each developmental stage were lettered anterior-to-posterior as in WormBook (McGhee, 2007) so that chromatin compactions in each specific intestinal cell could be compared between embryos. The exact intestinal cells with open arrays in each embryo were recorded and the percentages of open intestinal cells were calculated. Statistical analysis was performed by 2-way ANOVA using Prism Graph Pad.

Fluorescence In Situ Hybridization

Fluorescent probes were made by PCR labeling as described in Meister *et al*., 2013 using fluorescent 568-5-dUPT (Thermo Fisher C11399) and ULYSIS Nucleic Acid Labeling Kits using Alexa Fluor 488 (molecular probes life technologies U21650) (Primer sequences available in Table S3). Worm genomic DNA was used as the template to create five ~500bp probes ~50kbp upstream and downstream *pha-4*, *myo-3, ekl-1*, *coh-3*, and C05C10.7 loci. High temperature samples were collected by upshifting L4 P0 worms to 26°C before collecting F1 embryos. Embryos were dissected in 1X M9 on slides and then frozen in liquid nitrogen. After freeze-cracking, slides were fixed in methanol (on ice, 2 minutes) followed by 4% formaldehyde (4°C, 10 minutes) and then washed two times in 1X PBS (room temperature, 2 minutes). Embryos were permeabilized in 0.5% PBS-Triton X-100 (room temperature, 5 minutes), washed two times in 1XPBS (room temperature, 2 minutes), rinsed in 0.01 N HCl, and incubated in 0.1 N HCl (room temperature, 2 minutes). Slides were then washed once with 1X PBS

(room temperature, 3 minutes), once with 2X SSC (room temperature, 3 minutes) and then treated with 50 ug/mL of RNase A (VWR 1247C393) in 2X SSC for 45 minutes at 37°C by overlaying the sample with 500ul of RNAse solution and incubating in a humidified chamber. Slides were then washed once with 2X SSC (room temperature, 2 minutes), and then incubated in 2X SSC/50% formamide for 2 hours at room temperature. The probe was diluted to a concentration of 2-5 ng/µl in 100% deionized formamide and an equal volume of hybridization buffer was added. 25 µl of the probe solution was added to the sample, and overlayed with a glass chamber sealed with cement glue. The slides were pre-hybridized overnight at 37°C in a humidified chamber. FISH probe and sample were denatured at 76°C by placing the slides on a heat block, and then incubated for hybridization for 3 days at 37°C. Hybridization was followed by three washes of 2X SSC (37°C, 5 minutes) and two times in 0.2X SSC (55°C, 5 minutes). Images were captured using a Nikon A1R laser scanning confocal unit controlled by NIS-Elements fitted on a Nikon inverted Eclipse T*i-E* microscope with a Nikon DS-Qi1Mc camera and Plan Apo 100X/1.4 numerical aperture oil objective. Analysis was done using Metamorph isosurface function to determine the 3-D distance between the two centroids as described in Yuzyuk et al*.,* 2009. ND2 files were opened in Metamorph, a rectangular box was drawn around a single embryo, and the stack was opened in 4D viewer. Inclusive threshold and the isosuface function were used to create a mask of both probes. Each masked probe was selected and the X,Y and Z coordinate was calculated using the measure function to determine the centroid of the probe in 3D space. Statistical analysis was performed by 2-way ANOVA using Prism Graph Pad.

Embryo Shift Assays

For downshifting experiments: P0 L4 wildtype and mutant strains expressing *caIs79[elt-2p::dTomato, pRF4 (rol-6+)]* worms were upshifted to 26°C. The next day, 2-cell embryos were dissected out of adults in 1X M9, plated on NGM, and the plate was returned to 26°C. Developmental stages were determined based on the number of intestinal cells made visible by the *caIs79* transgene. Embryos were downshifted to 20°C when the majority of embryos on the plate were at 4E (~2 hours), 8E (~3 hours),

16E (~5 hours), comma (~7 hours), pretzel ~(9 hours), and L1 (~14 hours). The HTA phenotype was scored two days after shifting as described in Petrella et al., 2011. Each downshift was done 4-6 times with 10-20 embryos plated per replicate (n=55-77). For upshifting experiments a similar protocol was used: 2-cell embryos were dissected out of adults and maintained continually at 20°C. After dissection embryos were plated and kept at 20°C until being upshifted to 26°C at 4E, 8E, 16E, comma, pretzel, and L1 stage. Plates were scored for HTA two days after shifting. Each upshift was done 4-6 times with 10-20 embryos plated per replicate (n=58-101).

PGL expression analysis

P0 L4 wildtype and mutant strains expressing *caIs79[elt-2p::dTomato, pRF4 (rol-6+)]*; *pgl-1(sam33[pgl-1::gfp::3xFlag])* worms were upshifted to 26°C. The next day, adults were dissected in 1X M9 and 2-cell embryos placed in 1X M9 on polylysine coated slides in humid chambers and returned to 26°C. Embryos were downshifted on slides to 20°C at 8E, 16E, and comma stage. Arrested L1 larva were fixed in methanol and acetone and imaged in Z stack using a Nikon A1R laser scanning confocal unit controlled by NIS-Elements fitted on a Nikon inverted Eclipse T*i-E* microscope with a Nikon DS-Qi1Mc camera and Plan Apo 60X/1.2 numerical aperture oil objective. . Mean fluorescent intensity of PGL-1:GFP was determined using ImageJ. Statistical analysis was performed by 2-way ANOVA using Prism Graph Pad.

Embryonic Timing Assays

P0 L4 wildtype and mutant strains expressing *caIs79[elt-2p::dTomato, pRF4 (rol-6+)]* worms were placed at 20°C or 26°C. The next day, 2-cell embryos were dissected out of adults in 1X M9, plated on NGM, a timer was started, and the plate was returned to 20°C or 26°C. Plates were removed from the incubator and monitored for ~15 min at predetermined times based on approximate timing of stages known for each stage scored (8E, 16E, comma, pretzel, and L1). During the window the time each embryo within the population of ~10 embryos on the plate reached the specific development stage was recorded. The plate was then returned to the incubator and the process repeated for each subsequent stage. Developmental stages were determined based on

the number of intestinal cells in which *elt-2p::dTomato* expression was detected. n=20 embryos/condition.

MET-2::FLAG localization

Immunostaining of embryos was adapted from Strome and Wood 1983. Embryos were collected by picking gravid *3xFlag::met-2* adults (Mutlu et al., 2018) into 20 µl bubbles of 1X M9 on hydrophobic polylysine covered slides. Adults were dissected in half at the vulva site to release embryos from inside the worm. Samples were then overlaid with a coverslip, excess liquid was wicked away, and the slide was immersed in liquid nitrogen for at least 5 minutes. Slides were removed from liquid nitrogen, the coverslip was removed, and the samples were fixed in methanol at 4°C for 10 minutes and acetone at 4°C for 10 minutes. Slides were air dried and blocked for 30 minutes at room temperature. Slides were incubated with primary antibody for ~18 hours at 4°C, anti-FLAG (Sigma F1804-200ug) primary at a 1:100 dilution. Slides were washed two times in PBS for 10 minutes, blocked for 15 minutes at room temperature, and incubated with Alexa Fluor 488 (Invitrogen) secondary antibody at a 1:500 dilution and DAPI at a 1:500 dilution for 2 hours at room temperature. Slides were washed four times for 10 minutes each in PBS at room temperature and were mounted in Gelutol mounting media. Images were acquired with Nikon A1R laser scanning confocal controlled by NIS-Elements fitted on a Nikon inverted Eclipse T*i*-E microscope with a Nikon DS-Qi1Mc camera and Plan Apo 100X/1.4 numerical aperture oil objective.

Acknowledgments

Thanks to Jim McGhee for JM163, Eleanor Maine for EL634, and Dustin Updike for DUP75 strains. Some strains were provided by the CGC, which is funded by NIH Office of Research Infrastructure Programs (P40 OD010440). Many thanks to Anita Manogaran for comments and discussion of the manuscript.

Declaration of Interests

The authors declare no competing interests.

Funding

This work was supported by a NIH grants R00GM98436 and R15GM122005 to L.N.P.

References

Albertson, D., G., and Thomson, J.N. (1982) The kinetochores of *Caenorhabditis elegans. Chromosoma* **86**, 409-428.

Ahringer, J., and Gasser, S.M. (2018) Repressive Chromatin in *Caenorhabditis elegans:* Establishment, Composition, and Function. *Genetics* **208**, 491-511.

Andersen, E.C., Horvitz, H.R. (2007) Two C. elegans histone methyltransferases repress *lin-3* EGF transcription to inhibit vulval development. *Development* **134**, 2991-2999.

Andralojc, K.M., Campbell, A.C., Kelly, A.L., Terrey, M., Tanner, P.C., Gans, I.M., Senter-Zapata, M.J., Khokhar, E.S., and Updike, D.L. (2017) ELLI-1, a novel germline protein, modulates RNAi activity and P-granule accumulation in Caenorhabditis elegans.. *PLoS Genet* **12**, e1006611.

Ardizzi, JP., and Epstein, H.F. (1987) Immunochemical localization of myosin heavy chain isoforms and paramyosin in developmentally and structurally diverse muscle cell types of the nematode *Caenorhabditis elegans. J Cell Biol.* **105**, 2763-2770.

Begasse, M.L., Leaver, M., Vazquez, F., Grill, S.W., and Hyman, A.A. (2015) Temperature dependence of cell division timing accounts for a shift in the thermal limits of *C. elegans* and *C. briggsae. Cell Rep.* **10,** 647-653.

Ebata, K.T., and Mesh, K., Liu, S., Bilenky, M., Fekete, A., Acker, M.G., Hirst, M., Garcia, B.A., and Ramalho- Santos, M. (2017) Vitamin C induces specific demethylation of H3K9me2 in mouse embryonic stem cells via Kdm3a/b. *Epigenetics and Chromatin.* **10**, 36.

Elgin, S.C., and Reuter, G. (2013) Position-effect variegation, heterochromatin formation, and gene silencing in Drosophila. *Col Spring Harb Perspect Biol* **5**, a017780.

Evans, K.J., Huang, N., Stempor, P., Chesney, M.A., Down, T.A., and Ahringer, J. (2016) Stable *Caenorhabditis elegans* chromatin domains separate broadly expressed and developmentally regulated genes. *PNAS* **113,** E7020-E7029.

Fakhouri, T.H., Stevenson, J., Chisholm, A.D. and Mango, S.E. (2010) Dynamic chromatin organization during foregut development mediated by the organ selector gene PHA-4/FoxA. *PLoS Genet.* **6,** e1001060.

Fay, D., and Yochem, J. (2007) The synMuv genes of *Caenorhabditis elegans* in vulval development and beyond. *Dev Biol* **306**, 1-9.

Felix, MA., and Duveau, F. (2012) Population dynamics and habitat sharing of natural populations of *Caenorhabditis elegans* and *C. briggsae. BMC Biology* **10,** 59.

Frezal, L., and Felix, MA. (2015) *C. elegans* outside the Petri dish. *Elife* **4**, e05849.

Fukushige, T., Schroeder, D.F., Allen, F.L., Goszczynski, B., McGhee, J.D. (1996) Modulation of gene expression in the embryonic digestive tract of *C. elegans*. *Dev Biol* **178**, 276-288.

Gaertner, B., Johnston, J., Chen, K., Wallaschek, N., Paulson, A., Garruss, A.S., Gaudenz, K., Kumar, B.D., Krumlauf, R., and Zeitlinger, J. (2012) Poised RNA Polymerase II changes over developmental time and prepares genes for future expression. *Cell Rep* **2**, 1670-1683.

Gerstein, M.B., Lu, Z.J., Van Nostrand, E.L., Cheng, C., Arshinoff, B.I., Liu, T., Yip, K.Y., Robilotto, R., Rechsteiner, A., Ikegami, K., et al. (2010) Integrative analysis of the Caenorhabditis elegans genome by the modENCODE project. *Science* **330**, 1775-1787.

Goetsch, P.D., Garrigues, J.M., and Strome, S. (2017) Loss of the *Caenorhabditis elegans* pocket protein LIN-35 reveals MuvB's innate function as the repressor of DREAM target genes. *PLoS Genet* **13**, e1007088.

Gonzalez-Sandoval, A., Towbin, B.D., Kalck, V., Cablanca, D. S., Gaidatzis, D., Hauer, M. H., Geng, L., Wang, L., Yang, T., Wang, X., Zhao, K., and Gasser, S. M. (2015) Perinuclear anchoring of H3K9-Methylated Chromatin Stabilizes Induced Cell Fate in *C. elegans* Embryos. *Cell* **163**, 1333-1347.

Gure, A.O., Chua, R., Williamson, B., Gonen, M., Ferrera, C.A., Gnjatic, S., Ritter, G., Simpson, A.J.G., Chen, Y.-T., Old, L.J., et al. (2005). Cancer-Testis Genes Are Coordinately Expressed and Are Markers of Poor Outcome in Non-Small Cell Lung Cancer. *Clinical Cancer Research* **11**, 8055–8062.

Harrison, M.M., Ceol, C.J., Lu, X., and Horvitz, H.R. (2006) Some *C. elegans* class B synthetic multivulva proteins encode a conserved LIN-35 Rb-containing complex distinct from a NuRD-like complex. *PNAS* **103**, 16782-16787.

Hartmann-Goldstein, I. J. (1967) On the relationship between heterochromatization and variegation in Drosophila, with special reference to temperature-sensitive periods. *Genet Res* **10**, 143-159.

Horner, M.A., Quintin, S., Domeier, M.E., Kimble, J., Labouesse, M., and Mango, S.E. (1998) *pha-4,* an *HNF-3I* homolog, specifies pharyngeal organ identity in *Caenorhabditis elegans. Genes and Development* **12**, 1947-1952.

.

Kiontke, K.C., Felix, MA., Ailio, M., Rockman, M.V., Braendle, C., Penigault, JB., and Fitch, D. HA. (2011) A phylogeny and molecular barcodes for *Caenorhabditis,* with numerous new speciies from rotting fruits. *BMC Evolutionary Biology* **11,** 339.

Latorre, I., Chesney, M.A., Garrigues, J.M., Stempor, P., Appert, A., Francesconi, M., Strome, S., and Ahringer, J. (2015). The DREAM complex promotes gene body H2A.Z for target repression. *Genes Dev.* **29**:485-500.

Levin, M., Hashimshony, T., Wagner, F., and Yanai, I. (2012) Developmental milestones punctuate gene expression in the *Caenorhabditits* embryo. *Dev Cell* **22**, 1101-1108.

Lian, Y., Meng, L., Ding, P., and Sang, M. (2018). Epigenetic regulation of MAGE family in human cancer progression-DNA methylation, histone modification and non-coding RNAs. *Clinical Epigenetics*. **10**:115.

Lin, R., Hill, R.J., and Priess, J.R. (1998) POP-1 and anterior-posterior fate decisions in *C. elegans* embryos. *Cell* **92**, 229-239.

Liu, T., Rechsteiner, A., Egelhofer, T.A., Vielle, A., Latorre, I., Cheung, M.S., Ercan, S., Ikegami, K., Jensen, M., Kolasinska-Zwierz, P., et al. (2011) Broad chromosomal domains of histone modification patterns in *C. elegans*. *Genome Res* **21**, 227-236.

Litovchick, L., Sadasivam, S., Florens, L., Zhu, X., Swanson, S.K., Velmurugan, S., Chen, R., Washburn, M.P., Liu, X.S., and DeCaprio, J.A. (2007). Evolutionarily Conserved Multisubunit RBL2/p130 and E2F4 Protein Complex Represses Human Cell Cycle-Dependent Genes in Quiescence. *Molecular Cell* **26**, 539–551.

Maine, E.A., Westcott, J.W., Prechtl, A.M., Dang, T.T., Whitehurst, A.W., and Pearson, G.W. (2016) The cancer/testis antigens SPANX-A/C/D and CTAG2 promote breast cancer invasion. *Oncotarget* **7**, 14708– 14726.

McGhee, J.D. (2007) The *C. elegans* intestine. *WormBook.*

Mutlu, B., Chen, HM., Moresco, J.J., Orelo, B.D., Yang, B., Gaspar, J., Kepller-Ross, S., Yates III, J.R., Hall, D.H., Maine, E.M., and Mango, S.E. (2018) Regulated nuclear accumulation of a histone methyltransferase times the onset of heterochromatin formation in *C. elegans* embryos. *Sci Adv* **4**, eaat6224.

Petrella, L.N., Wang, W., Spike, C.A., Rechtsteiner, A., Reinke, V., and Strome, S. (2011) synMuv B proteins antagonize germline fate in the intestine and ensure *C. elegans* survival. *Development* **138**, 1069-1079.

Politz, J.C., Scalzo, D., and Groudine, M. (2013) Something silent this way forms: the functional organization of the repressive nuclear compartment. *Annu Rev Cell Dev Biol* **29**, 241-270.

Rechtsteiner, A., Costello, M.E., Egelhofer, T.A., Garrigues, J.M., Strome, S., and Petrella, L.N. (2019) Repression of germline genes in *Caenorhabditis elegans* somatic tissues by H3K9 Dimethylation of their promoters. *Genetics.* **12,**125-140.
Robertson, S., and Lin, R. (2015) The maternal-to-zygotic transition in *C. elegans*. *Curr Top Dev Biol* **113**,1-42.

Schulenburg, H., and Felix, MA. (2017) The natural biotic environment of *Caenorhabditis elegans*. *Genetics* **206,** 55-86.

Simon, J.A., and Kingson, R.E. (2013) Occupying chromatin: polycomb mechanisms for getting to genomic targets, stopping transcriptional traffic, and staying put. *Mol Cell* **49**, 808-824.

Schroeder, D.F., and McGhee, J.D. (1998) Anterior-posterior patterning within the *Caenorhabditis elegans* endoderm. *Development* **125**, 4877-4887.

Smolko, A.E., Shapiro-Kulnane, L., and Salz, H.K. (2018) The H3K9 methyltransferase SETDB1 maintains female identity in *Drosophila* germ cells. *Nat Commun* **9**, 4155.

Spencer, W.C., Zeller, G., Watson J.D., Henz, S.R., Watkins, K.L., McWhirter R.D., Petersen, S., Sreedharan, V.T., Widmer, C., Jo, J., et al. (2011) A spatial and temporal map of *C. elegans* gene expression. *Genome Res* **21**, 325-341.

Tabuchi, T. M., Deplancke, B., Osato, N., Zhu, L. J., Barrasa, M. I., Harrisons, M. M., Horvitz, H. R., Walhout, A. J. M., and Hagstrom, K. A. (2011) Chromosome-biased binding and gene regulation by the *Caenorhabditis elegans* DRM complex. *PLOS Genetics* **7**, 1-16.

Towbin, B. D., Gonzalez-Aguilera, C., Sack, R., Gaidatzis, D., Kalck, V., Meister, P., Askjaer, P., and Gasser, S.M. (2012) Step-wise methylation of histone H3K9 positions heterochromatin at the nuclear periphery. *Cell* **150**, 934-947.

Wang, D., Kennedy, S., Conte, D., Jr, Kim, J.K., Gabel, H.W., Kamath, R.S., Mello, C.C., and Ruvkun, G. (2005) Somatic misexpression of germline P granules and enhanced RNA interference in retinoblastoma pathway mutants. *Nature* **436**, 593-597.

Wu, X., Shi, Z., Cui, M., Han, M., and Ruvkin, G. (2012) Repression of germline RNAi pathways in somatic cells by retinoblastoma pathway chromatin complexes. *PLoS Genet* **8**, e1002418.

Xu, X., Tang, X., Lu, M., Tang, Q., Zhang, H., Zhu, H., Xu, N., Zhang, D., Xiong, L., Mao, Y., et al. (2014). Overexpression of MAGE-A9 predicts unfavorable outcome in breast cancer. *Experimental and Molecular Pathology* **97**, 579–584.

Yuzyuk, T., Fakhouri, T. H. I., Kiefer, J., and Mango, S. E. (2009) The polycomb complex protein *mes-2/E(z)* promotes the transition from developmental plasticity to differentiation in *C. elegans* embryos. *Dev. Cell* **16**, 699-710.

Zografos, B.R., and Sung, S. (2012) Vernalization-mediated chromatin changes. *Journal of Experimental Botany* **63**, 4343-4348.

Figures

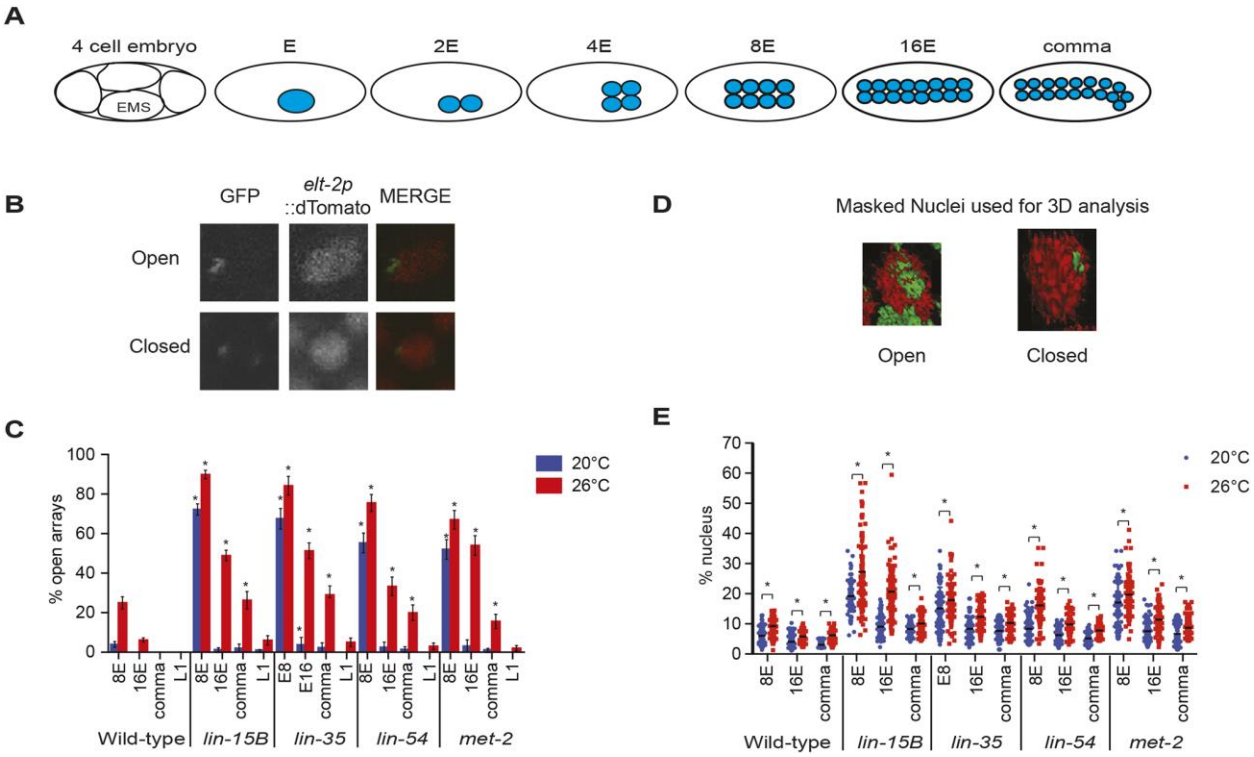

Figure 1: Loss of synMuv B proteins causes a delay in chromatin compaction in the intestinal lineage during development (A) A cartoon representing the number of intestinal cells and the approximate number of total cells in the stages scored throughout this study. (B) Representative images of intestinal nuclei with open and closed extrachromosomal arrays. (C) Intestinal nuclei were scored as open or closed based on array morphology (Yuzyuk et al., 2009) in worms raised at 20°C and 26°C at the 8E, 16E, comma, and L1 stage. Asterisks represent significant difference between the wild-type population at that stage and temperature ($p<0.01$, 2-way ANOVA). Error bars indicate standard error of the proportion. (C) The array volume to nuclear volume ratio was measured using the isosurface function in Metamorph at 8E, 16E, and comma at 20°C and 26°C. Each dot represents a single intestinal cell and the line represents the median. Asterisk represents a significant difference between 20°C and 26°C ($p<0.01$, 2-way Anova).

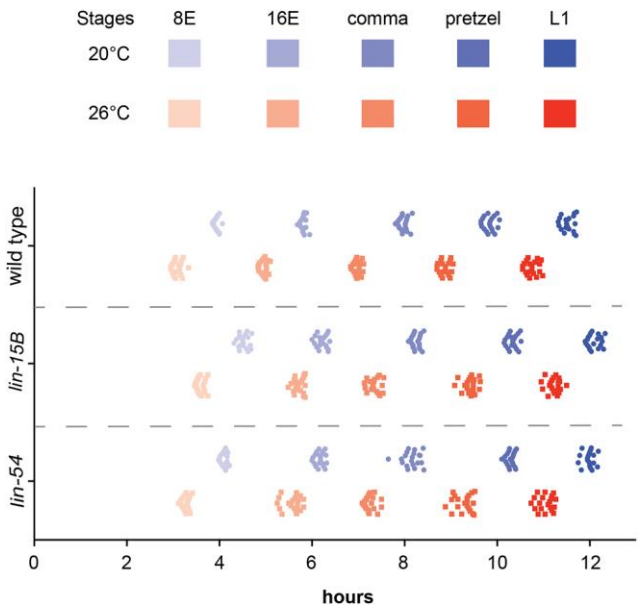

Figure 2: synMuv B mutants have delayed developmental timing compared to wild-type embryos Wild-type, *lin-15B,* and *lin-54* L4 P0 hermaphrodites were placed at 20°C or 26°C overnight. The next day, F1 two cell embryos were dissected, plated, and returned to the same temperature. The time to each intestinal stage for 8E, 16, comma, pretzel, and L1 was observed at recorded for each temperature. Each point represents an individual embryo (n=20 embryos/condition)

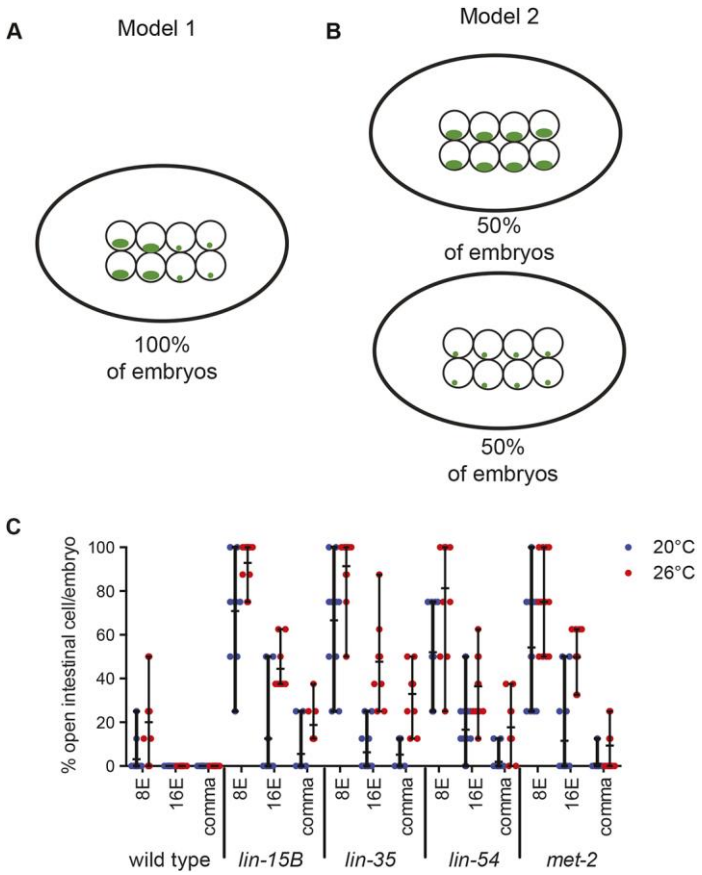

Figure 3: The number of intestinal cells with open chromatin varies within a single nucleus

Models that explain (A) a variance in compaction of intestinal cells within an embryo or (B) a variance in compaction of intestinal cells between different embryos. (C) The percentage of intestinal cells with an array in an open configuration per embryo was determined for 8E, 16E and comma stage embryos at 20°C and 26°C. Each dot represents an embryo and the line represents the mean percentage of open cells per embryo.

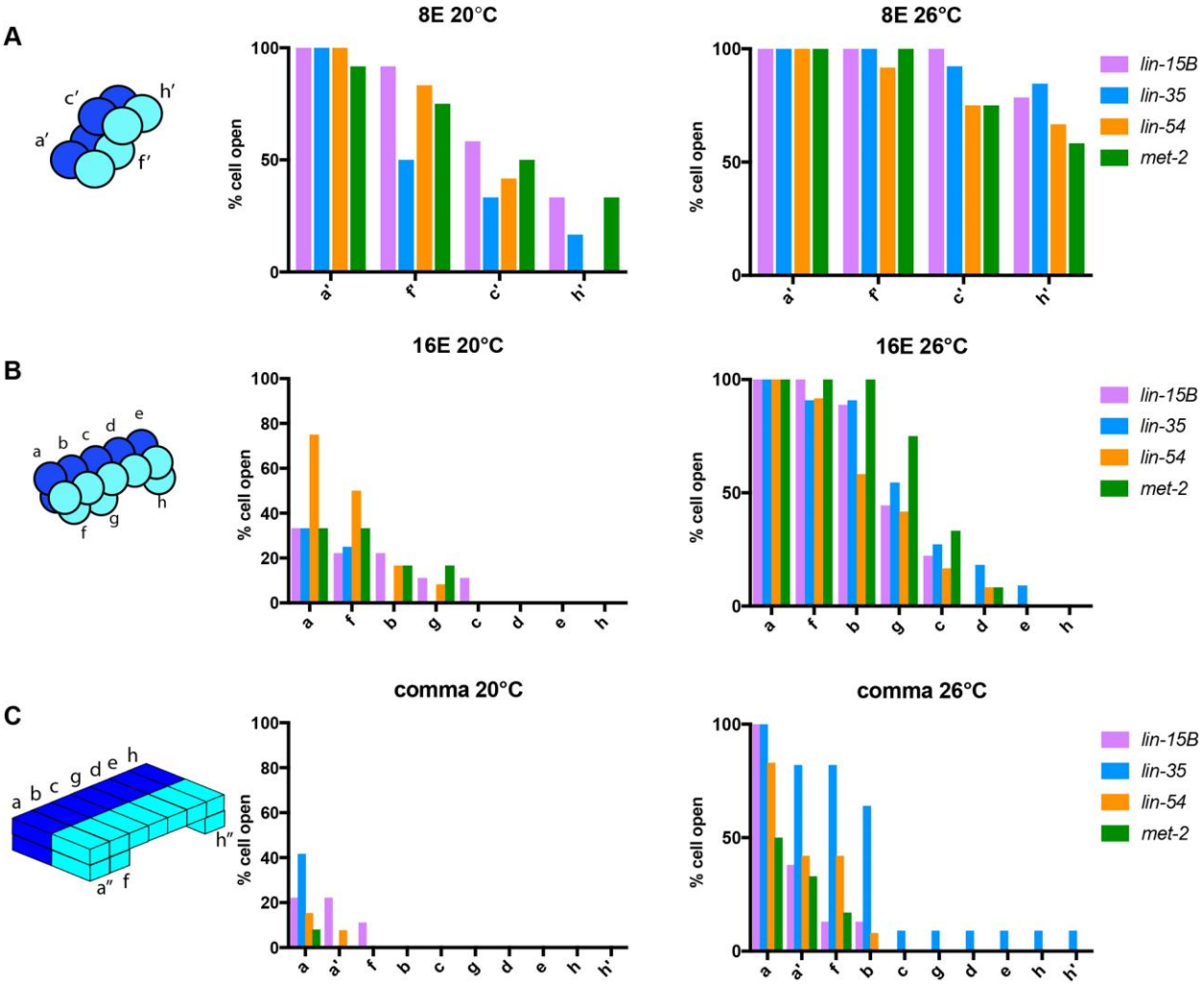

Figure 4: In synMuv B mutants anterior intestinal cells are more delayed in compaction than posterior intestinal cells

The position of open cells within a single embryo was monitored throughout development at (A) 8E, (B) 16E, and (C) 20E at both 20°C and 26°C. The anterior-to-posterior location of a cell was noted and that cell was recorded as having either an open or closed array. The percent of cells with open arrays for each pair of sister cells was plotted to in an anterior-to-posterior directionality.

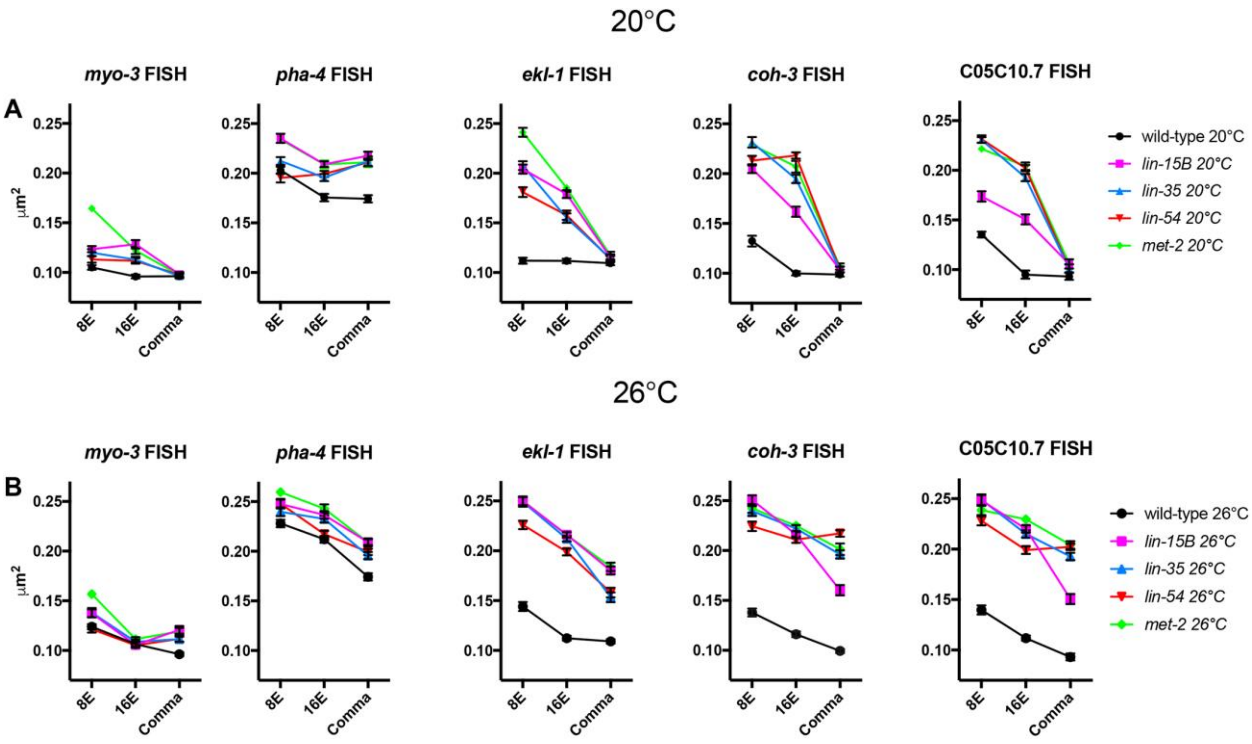

Figure 5: synMuv B regulated chromosomal loci are open chromatin in synMuv B mutants

8E, 16E, and comma stage wild-type, *lin-15B, lin-35, lin-54,* and *met-2* embryos at (A) 20°C and (B) 26°C were labeled with 568-5-dUTP (red) and Alexa Fluor 488 (green) probes 50kb upstream and 50kb downstream of *myo-3, pha-4, ekl-1, coh-3* and C05C10.7. Plots represent the distribution of 3-D-distances between centroids (μm^2). See also Figure S1

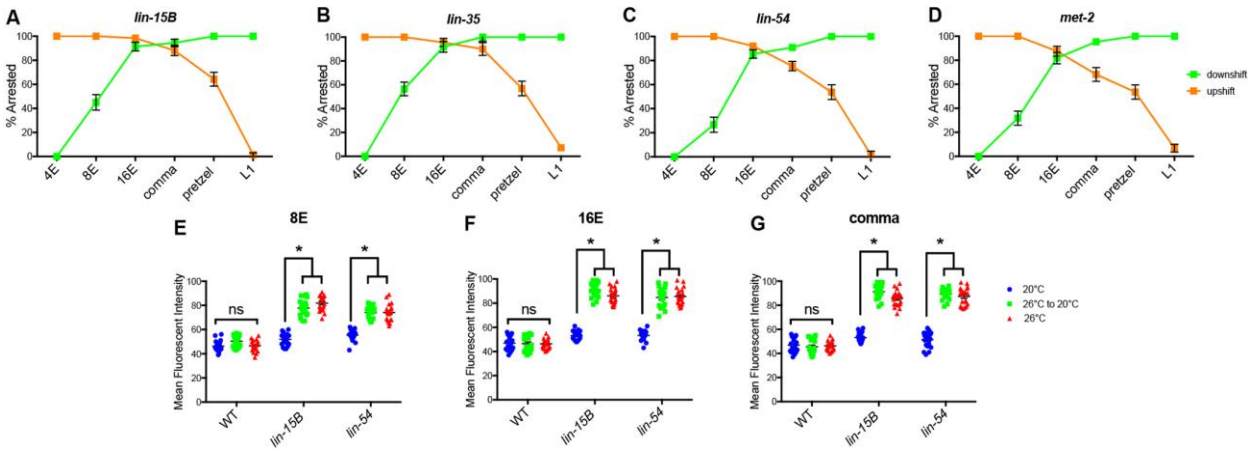

Figure 6: 16E through comma stage of embryogenesis is the temperature sensitive period crucial for larval HTA

(A-D) *lin-15B* (A)*, lin-35* (B), *lin-54* (C)*,* and *met-2* (D) L4 P0 hermaphrodites were placed at 20°C for upshift or 26°C for downshift experiments. Two cell embryos were dissected from P0s, and upshifted (red) or downshifted (blue) at 4E, 8E, 16E, comma, pretzel or L1 and scored for L1 larval arrest (n=60-78/point). (E-G) Mean Fluorescent Intensity of PGL-1 expression was determined for L1 wild-type, *lin-15B,* and *lin-54* embryos that were downshifted at 8E (E), 16E (F), comma (G) (n=20 L1/stage and temperature). ($p<0.01$, 2-way ANOVA). See also Figure S2

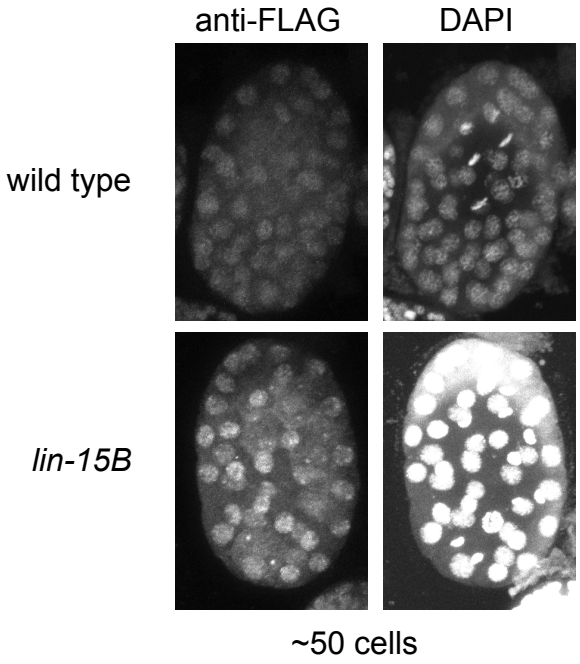

Figure S1: MET-2::FLAG accumulates in nuclei in *lin-15B* mutants by the ~50 cell stage similar to wild type
Wild type and *lin-15B* embryos expressing MET-2::FLAG at ~50 cell stage shown stained with anti-FLAG antibody and DAPI.

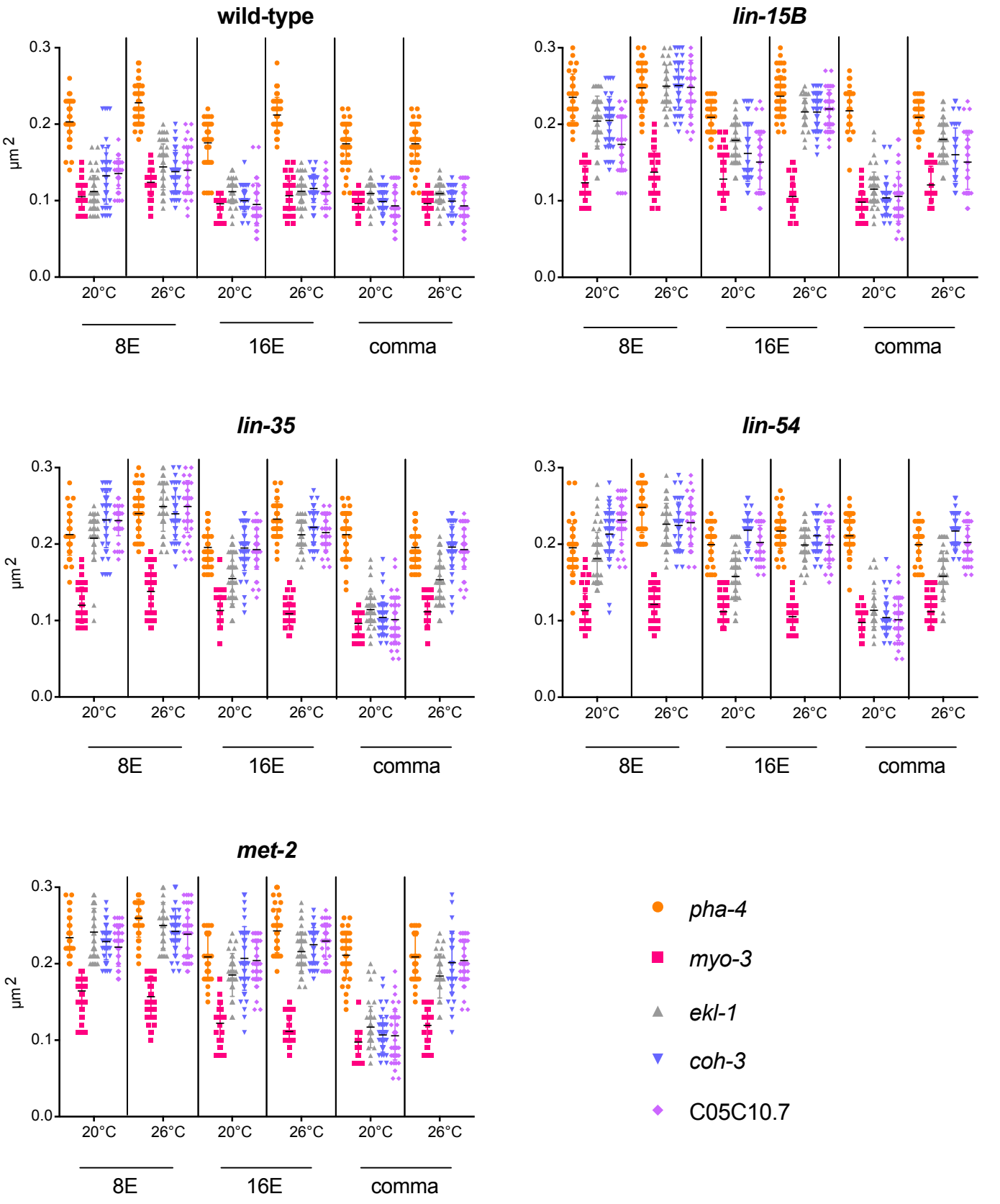

Figure S2 Related to Figure 4: Fluorescent in-situ hybridization of synMuv B regulated loci reveals more open chromatin in synMuv B mutants at higher temperatures

Wild-type (A), *lin-15B* (B), *lin-35* (D), *lin-54* (D), and *met-2* (E) embryos at 20°C and 26°C at 8E, 16E and comma stage were labeled with 568-5-dUTP (red) and Alexa Fluor 488 (green) probes 50kb upstream and 50kb downstream of *myo-3, pha-4, ekl-1, coh-3* and C05C10.7. Each dot represents the 3-D-distances between centroids (μm^2) of one intestinal cell.

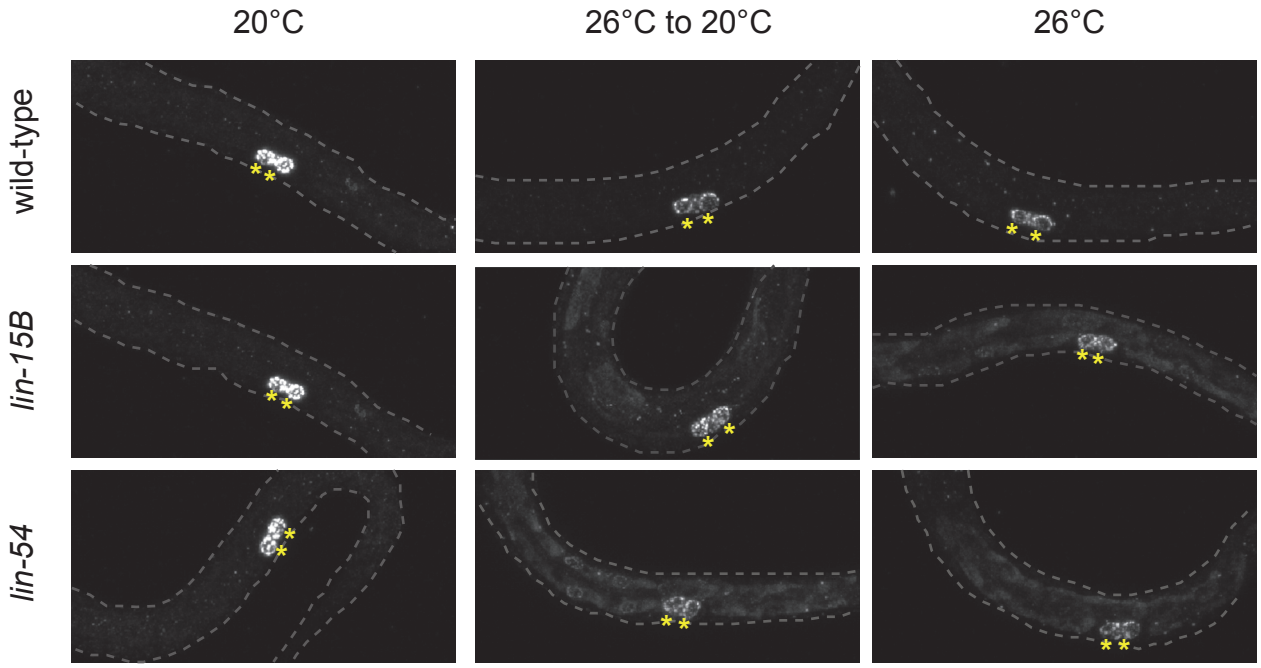

Figure S3 Related to Figure 5: synMuv B mutant embryos downshifted to low temperature at 16E ectopically express PGL-1

Wild-type, *lin-15B* mutant, and *lin-54* mutant embryos carrying a PGL-1:GFP transgene were placed at 26°C or 20°C in 1XM9 drops. Embryos were either kept at 26°C, downshifted to 20°C at 16E, or maintained at 20°C, and allowed to arrest at the L1 stage. L1 worms were fixed and imaged in Z-stack using confocal microscopy. Panels represent maximum projection of PGL-1:GFP. Asterisks mark primordial germ cells.

Table S1: Mean time to each intestinal developmental stage (min)

	wild-type		*lin-15B*		*lin-54*	
	20°C	**26°C**	**20°C**	**26°C**	**20°C**	**26°C**
2 cell - 8E	236	185	271	215	246	197
8E - 16E	349	297	373	342	372	334
16E - comma	479	418	495	440	491	434
comma - pretzel	590	531	619	564	619	555
pretzel - L1	691	644	725	672	720	661

Table S2: Difference in mean time to same genotype at 20°C to each intestinal developmental stage (min)

	wild-type		*lin-15B*		*lin-54*	
	20°C	**26°C**	**20°C**	**26°C**	**20°C**	**26°C**
2 cell - 8E	0	-51	0	-56	0	-49
8E - 16E	0	-52	0	-31	0	-38
16E - comma	0	-61	0	-55	0	-57
comma - pretzel	0	-59	0	-55	0	-64
pretzel - L1	0	-47	0	-53	0	-59

Table S3: Difference in mean time from wild type at same temperature to each intestinal developmental stage (min)

	wild-type		*lin-15B*		*lin-54*	
	20°C	**26°C**	**20°C**	**26°C**	**20°C**	**26°C**
2 cell - 8E	0	0	35	30	10	12
8E - 16E	0	0	24	45	23	37
16E - comma	0	0	16	22	12	16
comma - pretzel	0	0	29	33	29	24
pretzel - L1	0	0	34	28	29	17

Table S4: Strains used in this study

Strain Name	Genotype	Source
DUP0075	*pgl-1(sam33[pgl-1::gfp::3xFlag])*	Dustin Updike
EL634	*3XFlag::met-2*	Eleanor Maine
JM163	caIs79[elt-2p::dTomato, pRF4 (rol-6+)]	Jim McGhee
LNP0024	*lin-35(n745);* bnEx80(68XlacO +myo-3::mCherry+ worm genomic DNA); gwIs39[baf-1p::GFP::lacI::let-858 3\'UTR; vit-5::GFP]	This Study
LNP0026	*lin-54(n2231);* bnEx80(68XlacO +myo-3::mCherry+ worm genomic DNA); gwIs39[baf-1p::GFP::lacI::let-858 3\'UTR; vit-5::GFP]	This Study
LNP0027	*met-2(n4256);* bnEx80(68XlacO +myo-3::mCherry+ worm genomic DNA); gwIs39[baf-1p::GFP::lacI::let-858 3\'UTR; vit-5::GFP]	This Study
LNP0038	caIs79(elt-2p::dTomato;pRF4); *pgl-1(sam33[pgl-1::gfp::3xFlag])*	This Study
LNP0040	*lin-15B(n744)* bnEx80(68XlacO +myo-3::mCherry+ worm genomic DNA); gwIs39[baf-1p::GFP::lacI::let-858 3\'UTR; vit-5::GFP]; (caIs79(elt-2p::dTomato;pRF4))	This Study
LNP0041	*lin-15B(n744)* caIs79(elt-2p::dTomato;pRF4); *pgl-1(sam33[pgl-1::gfp::3xFlag])*	This Study
LNP0049	*lin-54(n2231)* caIs79(elt-2p::dTomato;pRF4); *pgl-1(sam33[pgl-1::gfp::3xFlag])*	This Study
LNP0050	bnEx80(68xlacO+myo-3::mCherry+worm genomic DNA); gwIs39[baf-1p::GFP::lacI::let-8583\'UTR;vit-5::GFP];caIs79(elt-2p::dTomato;pRF4))	This Study

Table S5: Primers used for DNA FISH

		Forward	Reverse
Upstream of *pha-4*	Pair 1	CGATGGAGCGCACTTGCACG	CAATCCCGGTAAAATGACG
	Pair 2	GGCAAACTGGTAAATTGTCGG	GCACCAGGCGCACTTTTGGC
	Pair 3	GCTGCTGGTTTTGACTGTGG	GGGTGAGTATCCAATTCCG
	Pair 4	CAACTCGTGATGACTTTAACC	GGTTGCACAGCCCTACATG
	Pair 5	GACTGAGTGAGATTGTAAAC	CTCGTATAAAGTTATTTCCCAGG
Dnstream of *pha-4*	Pair 1	CCAGCCACTGTGACATCGAC	CTTCAATGGTTAAACAAAGTTATG
	Pair 2	CTGATGCTAACCAAGAGAGTG	CATCGTCTAACTTTGAGCATAG
	Pair 3	CCTAACCGGTCAAATTTGTG	GCTAGAAGAATCAAGGCTTTTCC
	Pair 4	GTAATTGGTGGAAAAAGAAAATTTG	GCGGTCATTTTTCATATGCATCG
	Pair 5	CTCACTAACTTTCTCACAGAC	GTCTCGTTCAGCCACAAAAATTGC
Upstream of *myo-3*	Pair 1	CACCACCAACTCCCCCTTCT	GGTATATTTTCAATTGTGCC
	Pair 2	GCTTCATGGTAGATGGATTTG	CATTGCTCTCATTCCCACATGCTG
	Pair 3	GGATATAATTTCTTTGCAGGATC	GGCAATGAAACAACAACTTTTG
	Pair 4	CCAAGGTACGAGACATTTAC	GATGATATCAAGATTTTGAGAG
	Pair 5	GGCATGTATTTTCAGAAATATAC	GGATGTTATCAAAAGTTGAAG
Dnstream of *pha-4*	Pair 1	CCGCACACAAGTCTCAAATG	GGTGTCACAGAAATTCTATATTGG
	Pair 2	CGTTGATTTTACGAATCTTCCC	GCAATCAAGTCTAAACAATTTTTC
	Pair 3	CATAGAATTTGCTTACGTTTC	GATGAATTCACCCATTTCC
	Pair 4	GGACTTCTTCGATTGAG	GGCACAGTTTTAAGTGTTTCCG
	Pair 5	GTGGACATACATCAGCGTCAG	GTCTTGTTTCGGATCCTCATAAG
Upstream of *ekl-1*	Pair 1	GGGAGGGATTCTCAAAATCTTTC	GCAAGCTTTATTGGCAGATTCAG
	Pair 2	GGTTCTTAATTTTCTCTGAAAAAAGC	CGCGTGTCGTCGTTGGAGTTG
	Pair 3	CATGGCCTCCCTATTAGAAG	CCAAAATTGGGGGTTCCTCGAG
	Pair 4	CAAGTTTCAACAACACCGAATCC	GCTCTTTCAAATGTTGTTCAAGC
	Pair 5	GGATCATCTGCTGCTCCAACTCC	CCACTGGAGGTACAATTTTTACGC
Dnstream of *ekl-1*	Pair 1	CGAGTACCCCAAAAGCCGGC	GCCACATTACCAATAGTTTAGG
	Pair 2	GACGTGCCCAACATTGCC	CTGATAAAGTTTGCGCTCGG
	Pair 3	GCCACATGAGACACACACG	CTCCCAACAATGGTGCGCCTC
	Pair 4	CCGGGTACATCTCTCTGTTTC	GAGTTGAGCACACACATGG
	Pair 5	GCTGACATTGAACCGGATGAC	CGTCGCCTATCTTGCAATGG
Upstream of *coh-3*	Pair 1	GGTCATGTTGGACTAAATATAG	CCCGTTTTTCAAATTTATTTC
	Pair 2	GCAGAGATAAAGTGCTTATCATC	GGAGGTCAGCAATTAATATTTG
	Pair 3	GCAGACCTTTTCTTTTTCAC	CCAGGCACGTATAGACCAAGAACC
	Pair 4	GGGTGGCTGGTGACTTTGGAATGG	CCGACTCACTTCATTCCAAAC
	Pair 5	GCTCGGATTGCACGGATTGGCC	CTCACTTTCAGAATTAGAAC
Dnstream of *coh-3*	Pair 1	CCTCTTCTCTCTCTGTTCC	CACAACCTGAGCTTCTTGTTTATG
	Pair 2	GCGTCCCCTCCGTAAAGG	CTCGAATAAAAATGAAAACTTG
	Pair 3	CTGGAATCTGTGAAATGAATG	GTTGTACATAGTATGCCCTCG
	Pair 4	GTGGAGCAACCTATCCCC	GAAAAAATAGCTGACATTTTG
	Pair 5	GTCTTTATCCCGCCATTCTTCC	CTAATTGTTGGTTGTGAGG

Upstream of C05C10.7	Pair 1	CTAGCAGTATAAGTGTCAC	GACTTGAAGCTTGAAACGC
	Pair 2	GACTAAATTTATAACAACTTTATAG	GAGTAGCATCTCAGAACTG
	Pair 3	GGTATTCGGAAAACGGGTGAAACC	GTACTTGCAGTTTGCAGAAAG
	Pair 4	GACAAATGGCATCAAATATAG	GAAATCACAACAATTGAAATTCTG
	Pair 5	CCGATTAAGACCCGGACTTTAATTAC	CGACGAAAAGGAGAGACTCACTGG
Dnstream of C05C10.7	Pair 1	CCACAGAAAGTCCAATCTCG	CCTCGCGATTGTTGGGGAATC
	Pair 2	CGAGCCACTCAGCAAGGAAG	CAGCAACGTTGGCGAGTTCCTC
	Pair 3	CGTCTCATTGGAAAGGAGG	CGAGCCACTCAGCAAGGAAG
	Pair 4	GTAGGTATTGTTTGATTCGG	CGTGATGATCTTTTGGGATATCG
	Pair 5	GAGGTGGATGGAAAAAGAAG	GGAGCAAAAAAGATAGAGGAAG

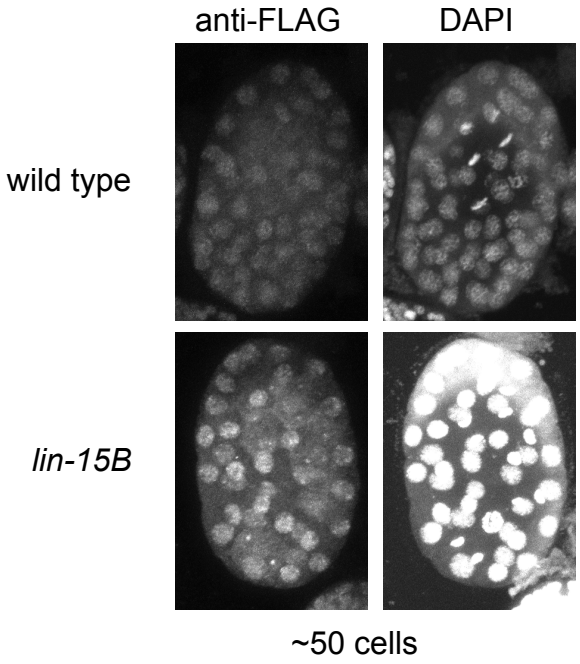

Figure S1: MET-2::FLAG accumulates in nuclei in *lin-15B* mutants by the ~50 cell stage similar to wild type
Wild type and *lin-15B* embryos expressing MET-2::FLAG at ~50 cell stage shown stained with anti-FLAG antibody and DAPI.

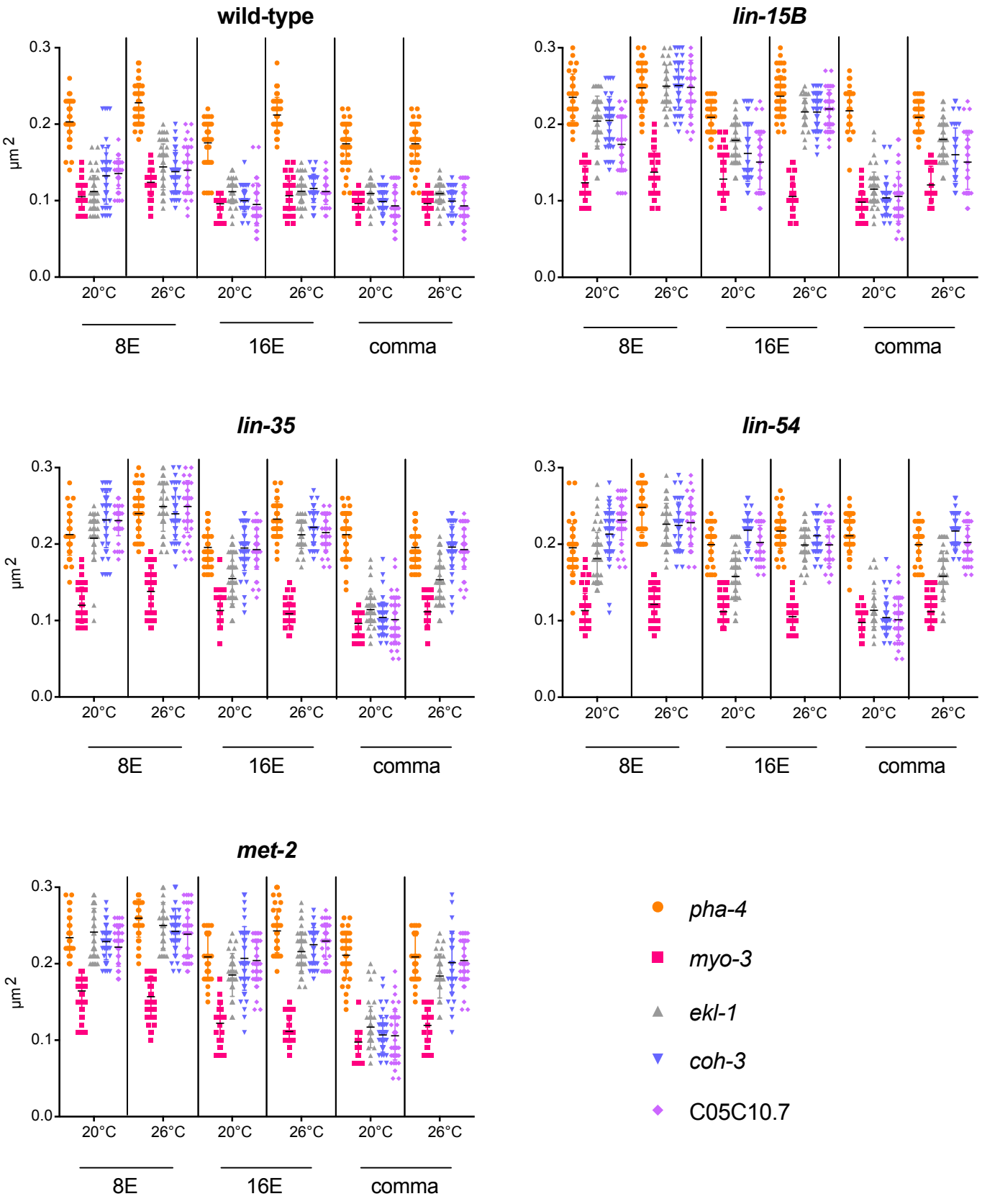

Figure S2 Related to Figure 4: Fluorescent in-situ hybridization of synMuv B regulated loci reveals more open chromatin in synMuv B mutants at higher temperatures

Wild-type (A), *lin-15B* (B), *lin-35* (D), *lin-54* (D), and *met-2* (E) embryos at 20°C and 26°C at 8E, 16E and comma stage were labeled with 568-5-dUTP (red) and Alexa Fluor 488 (green) probes 50kb upstream and 50kb downstream of *myo-3, pha-4, ekl-1, coh-3* and C05C10.7. Each dot represents the 3-D-distances between centroids (μm^2) of one intestinal cell.

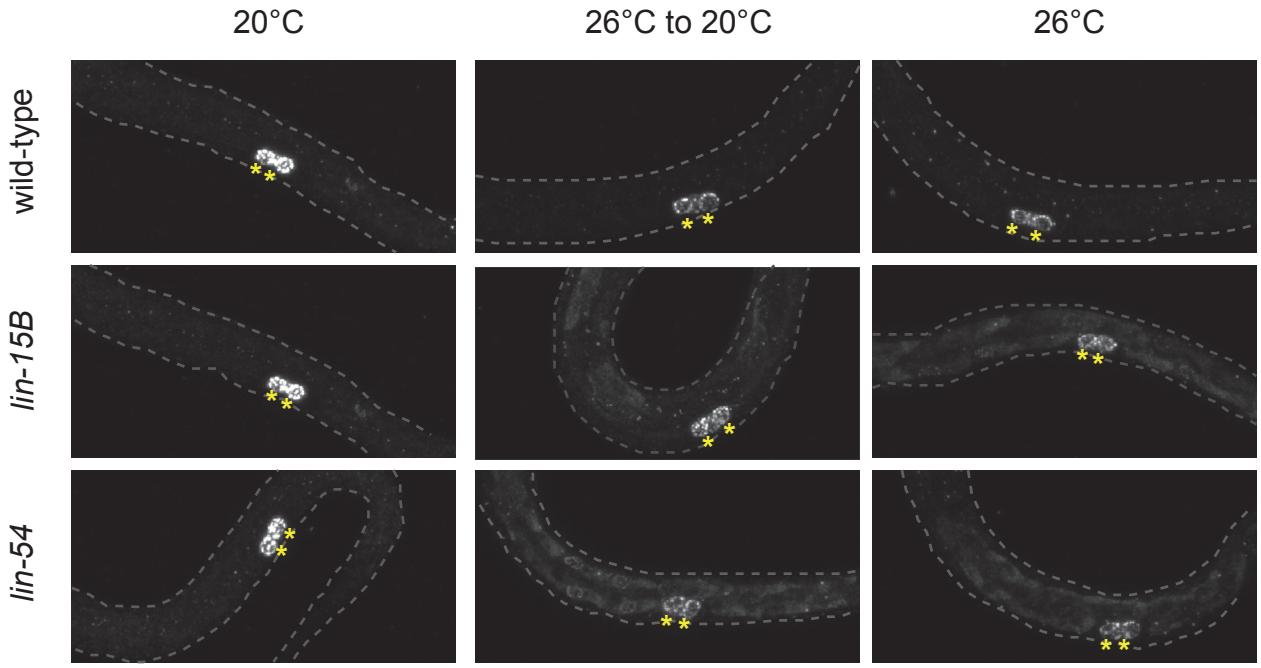

Figure S3 Related to Figure 5: synMuv B mutant embryos downshifted to low temperature at 16E ectopically express PGL-1

Wild-type, *lin-15B* mutant, and *lin-54* mutant embryos carrying a PGL-1:GFP transgene were placed at 26°C or 20°C in 1XM9 drops. Embryos were either kept at 26°C, downshifted to 20°C at 16E, or maintained at 20°C, and allowed to arrest at the L1 stage. L1 worms were fixed and imaged in Z-stack using confocal microscopy. Panels represent maximum projection of PGL-1:GFP. Asterisks mark primordial germ cells.

Table S1: Mean time to each intestinal developmental stage (min)

	wild-type		*lin-15B*		*lin-54*	
	20°C	**26°C**	**20°C**	**26°C**	**20°C**	**26°C**
2 cell - 8E	236	185	271	215	246	197
8E - 16E	349	297	373	342	372	334
16E - comma	479	418	495	440	491	434
comma - pretzel	590	531	619	564	619	555
pretzel - L1	691	644	725	672	720	661

Table S2: Difference in mean time to same genotype at 20°C to each intestinal developmental stage (min)

	wild-type		*lin-15B*		*lin-54*	
	20°C	**26°C**	**20°C**	**26°C**	**20°C**	**26°C**
2 cell - 8E	0	-51	0	-56	0	-49
8E - 16E	0	-52	0	-31	0	-38
16E - comma	0	-61	0	-55	0	-57
comma - pretzel	0	-59	0	-55	0	-64
pretzel - L1	0	-47	0	-53	0	-59

Table S3: Difference in mean time from wild type at same temperature to each intestinal developmental stage (min)

	wild-type		*lin-15B*		*lin-54*	
	20°C	**26°C**	**20°C**	**26°C**	**20°C**	**26°C**
2 cell - 8E	0	0	35	30	10	12
8E - 16E	0	0	24	45	23	37
16E - comma	0	0	16	22	12	16
comma - pretzel	0	0	29	33	29	24
pretzel - L1	0	0	34	28	29	17

Table S4: Strains used in this study

Strain Name	Genotype	Source
DUP0075	*pgl-1(sam33[pgl-1::gfp::3xFlag])*	Dustin Updike
EL634	*3XFlag::met-2*	Eleanor Maine
JM163	caIs79[elt-2p::dTomato, pRF4 (rol-6+)]	Jim McGhee
LNP0024	*lin-35(n745);* bnEx80(68XlacO +myo-3::mCherry+ worm genomic DNA); gwIs39[baf-1p::GFP::lacI::let-858 3\'UTR; vit-5::GFP]	This Study
LNP0026	*lin-54(n2231);* bnEx80(68XlacO +myo-3::mCherry+ worm genomic DNA); gwIs39[baf-1p::GFP::lacI::let-858 3\'UTR; vit-5::GFP]	This Study
LNP0027	*met-2(n4256);* bnEx80(68XlacO +myo-3::mCherry+ worm genomic DNA); gwIs39[baf-1p::GFP::lacI::let-858 3\'UTR; vit-5::GFP]	This Study
LNP0038	caIs79(elt-2p::dTomato;pRF4); *pgl-1(sam33[pgl-1::gfp::3xFlag])*	This Study
LNP0040	*lin-15B(n744)* bnEx80(68XlacO +myo-3::mCherry+ worm genomic DNA); gwIs39[baf-1p::GFP::lacI::let-858 3\'UTR; vit-5::GFP]; (caIs79(elt-2p::dTomato;pRF4))	This Study
LNP0041	*lin-15B(n744)* caIs79(elt-2p::dTomato;pRF4); *pgl-1(sam33[pgl-1::gfp::3xFlag])*	This Study
LNP0049	*lin-54(n2231)* caIs79(elt-2p::dTomato;pRF4); *pgl-1(sam33[pgl-1::gfp::3xFlag])*	This Study
LNP0050	bnEx80(68xlacO+myo-3::mCherry+worm genomic DNA); gwIs39[baf-1p::GFP::lacI::let-8583\'UTR;vit-5::GFP];caIs79(elt-2p::dTomato;pRF4))	This Study

Table S5: Primers used for DNA FISH

		Forward	Reverse
Upstream of *pha-4*	Pair 1	CGATGGAGCGCACTTGCACG	CAATCCCGGTAAAATGACG
	Pair 2	GGCAAACTGGTAAATTGTCGG	GCACCAGGCGCACTTTTGGC
	Pair 3	GCTGCTGGTTTTGACTGTGG	GGGTGAGTATCCAATTCCG
	Pair 4	CAACTCGTGATGACTTTAACC	GGTTGCACAGCCCTACATG
	Pair 5	GACTGAGTGAGATTGTAAAC	CTCGTATAAAGTTATTTCCCAGG
Dnstream of *pha-4*	Pair 1	CCAGCCACTGTGACATCGAC	CTTCAATGGTTAAACAAAGTTATG
	Pair 2	CTGATGCTAACCAAGAGAGTG	CATCGTCTAACTTTGAGCATAG
	Pair 3	CCTAACCGGTCAAATTTGTG	GCTAGAAGAATCAAGGCTTTTCC
	Pair 4	GTAATTGGTGGAAAAAGAAAATTTG	GCGGTCATTTTTCATATGCATCG
	Pair 5	CTCACTAACTTTCTCACAGAC	GTCTCGTTCAGCCACAAAAATTGC
Upstream of *myo-3*	Pair 1	CACCACCAACTCCCCCTTCT	GGTATATTTTCAATTGTGCC
	Pair 2	GCTTCATGGTAGATGGATTTG	CATTGCTCTCATTCCCACATGCTG
	Pair 3	GGATATAATTTCTTTGCAGGATC	GGCAATGAAACAACAACTTTTG
	Pair 4	CCAAGGTACGAGACATTTAC	GATGATATCAAGATTTTGAGAG
	Pair 5	GGCATGTATTTTCAGAAATATAC	GGATGTTATCAAAAGTTGAAG
Dnstream of *pha-4*	Pair 1	CCGCACACAAGTCTCAAATG	GGTGTCACAGAAATTCTATATTGG
	Pair 2	CGTTGATTTTACGAATCTTCCC	GCAATCAAGTCTAAACAATTTTTC
	Pair 3	CATAGAATTTGCTTACGTTTC	GATGAATTCACCCATTTCC
	Pair 4	GGACTTCTTCGATTGAG	GGCACAGTTTTAAGTGTTTCCG
	Pair 5	GTGGACATACATCAGCGTCAG	GTCTTGTTTCGGATCCTCATAAG
Upstream of *ekl-1*	Pair 1	GGGAGGGATTCTCAAAATCTTTC	GCAAGCTTTATTGGCAGATTCAG
	Pair 2	GGTTCTTAATTTTCTCTGAAAAAAGC	CGCGTGTCGTCGTTGGAGTTG
	Pair 3	CATGGCCTCCCTATTAGAAG	CCAAAATTGGGGGTTCCTCGAG
	Pair 4	CAAGTTTCAACAACACCGAATCC	GCTCTTTCAAATGTTGTTCAAGC
	Pair 5	GGATCATCTGCTGCTCCAACTCC	CCACTGGAGGTACAATTTTTACGC
Dnstream of *ekl-1*	Pair 1	CGAGTACCCCAAAAGCCGGC	GCCACATTACCAATAGTTTAGG
	Pair 2	GACGTGCCCAACATTGCC	CTGATAAAGTTTGCGCTCGG
	Pair 3	GCCACATGAGACACACACG	CTCCCAACAATGGTGCGCCTC
	Pair 4	CCGGGTACATCTCTCTGTTTC	GAGTTGAGCACACACATGG
	Pair 5	GCTGACATTGAACCGGATGAC	CGTCGCCTATCTTGCAATGG
Upstream of *coh-3*	Pair 1	GGTCATGTTGGACTAAATATAG	CCCGTTTTTCAAATTTATTTC
	Pair 2	GCAGAGATAAAGTGCTTATCATC	GGAGGTCAGCAATTAATATTTG
	Pair 3	GCAGACCTTTTCTTTTTCAC	CCAGGCACGTATAGACCAAGAACC
	Pair 4	GGGTGGCTGGTGACTTTGGAATGG	CCGACTCACTTCATTCCAAAC
	Pair 5	GCTCGGATTGCACGGATTGGCC	CTCACTTTCAGAATTAGAAC
Dnstream of *coh-3*	Pair 1	CCTCTTCTCTCTCTGTTCC	CACAACCTGAGCTTCTTGTTTATG
	Pair 2	GCGTCCCCTCCGTAAAGG	CTCGAATAAAAATGAAAACTTG
	Pair 3	CTGGAATCTGTGAAATGAATG	GTTGTACATAGTATGCCCTCG
	Pair 4	GTGGAGCAACCTATCCCC	GAAAAAATAGCTGACATTTTG
	Pair 5	GTCTTTATCCCGCCATTCTTCC	CTAATTGTTGGTTGTGAGG

Upstream of C05C10.7	Pair 1	CTAGCAGTATAAGTGTCAC	GACTTGAAGCTTGAAACGC
	Pair 2	GACTAAATTTATAACAACTTTATAG	GAGTAGCATCTCAGAACTG
	Pair 3	GGTATTCGGAAAACGGGTGAAACC	GTACTTGCAGTTTGCAGAAAG
	Pair 4	GACAAATGGCATCAAATATAG	GAAATCACAACAATTGAAATTCTG
	Pair 5	CCGATTAAGACCCGGACTTTAATTAC	CGACGAAAAGGAGAGACTCACTGG
Dnstream of C05C10.7	Pair 1	CCACAGAAAGTCCAATCTCG	CCTCGCGATTGTTGGGGAATC
	Pair 2	CGAGCCACTCAGCAAGGAAG	CAGCAACGTTGGCGAGTTCCTC
	Pair 3	CGTCTCATTGGAAAGGAGG	CGAGCCACTCAGCAAGGAAG
	Pair 4	GTAGGTATTGTTTGATTCGG	CGTGATGATCTTTTGGGATATCG
	Pair 5	GAGGTGGATGGAAAAAGAAG	GGAGCAAAAAAGATAGAGGAAG